

# Effects of water droplet evaporation on initiation, propagation and extinction of premixed spherical flames

Yijie Zhuang, Huangwei Zhang\*

Department of Mechanical Engineering, National University of Singapore, 9 Engineering Drive 1, 117576 Singapore

## ARTICLE INFO

### Article history:

Received 4 February 2019

Revised 24 April 2019

Accepted 10 May 2019

Available online 11 May 2019

### Keywords:

Water droplet evaporation

Heat loss

Flame ignition

Flame propagation

Minimum ignition energy

## ABSTRACT

In this study, we develop a simplified theoretical model for flame initiation, propagation and extinction in premixed gas mixture containing water droplets, by considering water droplet evaporation in pre-flame or/and post-flame zones. The Eulerian droplet model with simplified evaporation sub-model is employed, while for gas phase the assumptions of constant-density, quasi-steady and large activation energy are made. Analytical correlations describing different flame regimes and transitions among flame balls, propagating spherical flames and planar flames are then derived to investigate the spherical flame initiation, propagation and extinction, with emphasis on the effects of water droplet evaporation on spherical flames at different Lewis numbers. Five different flame regimes are observed and discussed for droplets evaporation in pre-flame or/and post-flame zones. It is found that the droplets with larger heat exchange coefficient are more effective in reducing flame propagation speed and temperature but increasing the vaporization front. Moreover, the cooling effect of evaporation heat loss plays an important role on flame regimes and their transitions. At the relatively large heat exchange coefficient, the total evaporation heat loss from pre-flame and post-flame zones reaches its maximum at an intermediate flame radius. The cooling effect is strong enough to quench the flame and results in the self-extinguishing flame. In addition, the combined effects of stretch rate and Lewis number compete with the evaporation heat loss from droplet evaporation. For small Lewis number, the flammability limits can be achieved through self-extinguishing flames, whereas for large Lewis number the flames approach their flammability limits in their evolution into planar flames. For ignition of spherical flames, if the droplet-laden mixture is intrinsically non-flammable, although a propagating flame kernel can be initiated, however it would still be quenched due to evaporation heat loss at a critical radius. The minimum ignition energy increases with heat exchange coefficient and Lewis number.

© 2019 Elsevier Ltd. All rights reserved.

## 1. Introduction

Evaporation of water droplets in combustion systems has attracted many researchers' attentions for decades, because it renders us the possibility to actively affect or control the host reaction system of practical interest, like in fire suppression for civil infrastructures (e.g. buildings) and also space vehicles (e.g. manned spaceships) (Grant et al., 2000). It is well known that water mist is an effective fire-suppression agent and has been developed for commercial practice.

Scientifically, droplet-laden combustion can be categorized as two-phase multi-component reacting flow problem and therefore the comprehensive interactions between continuous gas phase and dispersed liquid phase can be interpreted in terms of inter-phasic

exchanges of mass, momentum, energy and chemical species (Crowe et al., 2011). The interpretation for their coupling can be made based on the chemical, physical and thermal effects from the dispersed water droplets (Lentati and Chelliah, 1998a; Mitani, 1982). Specifically, the thermal effects are characterized mainly through the continuous absorption of the energy from the gas phase by the evaporating water droplets, and also through the convective heat transfer due to the inter-phasic temperature difference. The significant manifestation of the physical effects is dilution (or termed as "oxygen displacement"), due to the addition of the water vapour to the gaseous mixture. The direct consequences from dilution are variations of the local equivalence ratio, and also the mixture properties (e.g. density and heat capacity). Loosely, the thermal effects can also be viewed as one of the physical effects. Regarding the chemical effects, the water droplet can inhibit or promote the homogeneous chemical reaction pathways somehow. For instance, water vapour is expected to have higher three-body collision efficiency compared to other species (e.g. nitrogen), and

\* Corresponding author.

E-mail addresses: [mpezhuan@nus.edu.sg](mailto:mpezhuan@nus.edu.sg) (Y. Zhuang), [huangwei.zhang@nus.edu.sg](mailto:huangwei.zhang@nus.edu.sg) (H. Zhang).

## Nomenclature

$A$	pre-exponential factor of Arrhenius law
$C_p$	gas heat capacity
$d$	droplet diameter
$D$	gas molecular diffusivity
$D_{th}$	gas thermal diffusivity
$E$	activation energy
$l_{th}$	flame thickness of an adiabatic planar flame
$Le$	Lewis number
$m$	mass
$N_d$	droplet number density
$q_v$	latent heat of vaporization
$q_c$	chemical reaction heat release
$Q$	ignition energy
$R^0$	universal gas constant
$R_f$	flame radius
$R_v$	vaporization front
$s_d$	droplet surface area
$t, r$	temporal and spatial coordinates
$T$	temperature
$T_b$	flame temperature of an adiabatic planar flame
$T_v$	boiling point
$u_b$	laminar flame speed of an adiabatic planar flame
$U$	flame propagation speed
$Y$	gas mass fraction
$Y_d$	droplet mass loading
$Z$	Zel'dovich number

### Greek letters

$\rho_g$	gas density
$\omega_v$	droplet evaporation rate
$\omega_c$	chemical reaction rate
$\lambda_g$	gas heat conductivity
$\eta$	moving coordinate attached to the propagating flame front
$\eta_v$	location of vaporization front in the moving coordinate
$\Omega$	heat exchange coefficient
$\sigma$	thermal expansion ratio
$\delta$	initial droplet mass loading

### Superscripts

$\sim$	dimensional quantity
--------	----------------------

### Subscripts

$d$	corresponding to the liquid phase
$f$	at the flame front
$g$	corresponding to the gas phase
$v$	at the front of onset vaporization
$0$	in the fresh mixture

hence enhances the radical recombination, which further weakens the combustion process (Lentati and Chelliah, 1998a). Overall, the chemical effects from the dispersed water droplets are relatively minor, compared to the other two (Lentati and Chelliah, 1998a; Seshadri, 1978).

There have been numerous investigations available on water-droplet-laden combustion, and most of them are concentrated on understanding weakening (or “suppression” in fire science) of the gaseous flames caused by the dispersed water droplets. The experimental studies, for instance, rely on counterflow diffusion flames (Naito et al., 2011; Sasongko et al., 2011; Yoshida et al., 2015; Zegers et al., 2000), counterflow spray (*n*-heptane) diffusion flames (Sasongko et al., 2016), propane/air co-flowing diffusion flames (Sakurai et al., 2013), spherical hydrogen/air/steam pre-

mixed flames (Cheikhrravat et al., 2015) and premixed methane/air flames stabilized in nozzle-type burners (Fuss et al., 2002). It is found that water mist is more effective than inert agents (e.g. nitrogen) in reducing the burning velocity (Fuss et al., 2002). Also, addition of water droplets into the air stream can decrease the extinction strain rate in counterflow configurations (Naito et al., 2011; Yoshida et al., 2015). Meanwhile, the higher surface area parameter, the smaller extinction strain rate. The optimum droplet size is also identified, below which the flame suppression efficiency (e.g. reduction of burning velocity or extinction strain rate) is not improved with decreased droplet diameter. These findings are also confirmed by the numerical simulations of freely propagating hydrogen-, methane- and propane-air flames laden with water droplets made by Kee and his co-workers (Modak et al., 2006; Yang and Kee, 2002). Based on their results, the optimum size for reducing the burning velocity is about 2  $\mu\text{m}$  for hydrogen, while it is around 10  $\mu\text{m}$  for methane and propane. The optimum droplet size determined from the non-premixed counterflow methane flames is in the range of 15–20  $\mu\text{m}$  (Chelliah, 2007; Lentati and Chelliah, 1998b, 1998a).

Besides the above investigations based on the specific experimental measurements and numerical computations, there are also theoretical analyses on droplet-laden flames available. Greenburg and Dvorjetski investigate the effects of polydispersed water spray on extinction of counterflow polydispersed spray flame and gaseous diffusion flames (Dvorjetski and Greenberg, 2004, 2002). In their work, the effects of spray polydispersity on optimal flame suppression conditions are highlighted. Additionally, the multiplicity and bifurcation of flame propagation velocity is observed when the particle or droplet properties (e.g. diameter, initial loading, etc.) are varied (Belyakov et al., 2018; Mitani, 1981; Blouquin and Joulin, 1998). However, to the best of our knowledge, there are still limited analytical studies on the transient development of droplet-laden flames about their initiation, propagation and extinction. This, in reality, can help us examine the comprehensive effects of the dispersed water droplets on various regimes or stages of the evolving flames.

The propagating spherical gaseous flames have been extensively adopted to understand flame initiation and propagation, because of their geometrical simplicity, e.g. in Chen (2010); Chen et al. (2011, 2009); Chen and Ju (2007); He (2000); Zhang et al. (2013a, 2013b); Zhang and Chen (2011). For multi-phase spherical flames, Greenberg (2007) derives an evolution equation to evaluate the finite-rate evaporation and droplet drag effects for the first time. Han and Chen (2015) investigate the effects of finite-rate droplet evaporation on ignition and propagation of premixed spherical spray flame. They also use the similar method to examine the effects of finite-rate droplet evaporation on extinction of spherical burner-stabilized diffusion flames (Han and Chen, 2016). The above studies unveil interesting results regarding the effects of fuel droplet evaporation on initiation, propagation and extinction of propagating spherical flames.

The present work aims to conduct the mathematical analysis on premixed spherical flame initiation, propagation and extinction in the combustible gas mixture with water droplets. The focus is on finding general theoretical descriptions of different flame regimes and transitions among the ignition kernels, flame balls, propagating spherical flames and planar flames. The effects of droplet evaporation and Lewis number on flame propagation speed, vaporization front, extinction, and minimum ignition energy will be examined. The rest of the paper is structured as below. Mathematical model and theoretical analysis are presented in Sections 2 and 3, respectively. Results from the theoretical analysis will be discussed in detail in Section 4. Section 5 closes the paper with the main conclusions.

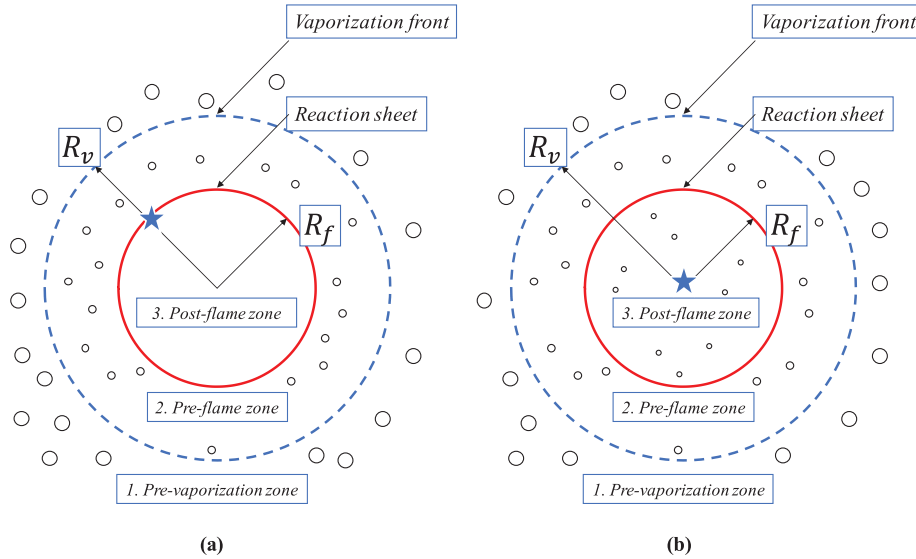


**Fig. 1.** Schematic of the problem studied in (a) Case 1 and (b) Case 2. The star symbols in (a) and (b) represent the locations where the droplets completely vaporize, i.e. in the reaction sheet and spherical centre, respectively.

## 2. Mathematical model

We consider a simplified model for initiation and propagation of one-dimensional laminar spherical premixed flame laden with water droplets. Our model includes three different regions to describe droplet evaporation and fuel combustion (Greenberg, 2007; Greenberg et al., 1993; Han and Chen, 2015). As shown in Fig. 1, the flame structure consists of a pre-vaporization zone (Zone 1), a pre-flame zone (Zone 2), and a post-flame zone (Zone 3). The above three zones are respectively demarcated by the vaporization front (dashed lines in Fig. 1) and flame front (solid lines in Fig. 1). Note that the vaporization front  $R_v$  corresponds to the location where the droplet starts to evaporate. Various distributions of water droplets may be presented in practical situations, depending on the droplet characteristics (e.g. diameter and mass loading) and evaporation rate (Belyakov et al., 2018). For instance, it is difficult for small water droplets to penetrate through the flame and they are fully vaporized before the flame front  $R_f$ . Nevertheless, for large droplets, they can survive for a longer time and vaporize in both unburned and burned zones (Yang and Kee, 2002). As such, in the current work, two cases (termed as Case 1 and Case 2) are investigated to examine the effects of droplet evaporation in different zones on initiation and propagation of spherical flames. Specifically, in Case 1, as shown in Fig. 1a, the water droplets are completely vaporized before the flame front, whereas in Case 2 (Fig. 1b), they pass the flame front and continue to vaporize in the post-flame zone. In other words, for Case 1, evaporation occurs only in Zone 2, whilst for Case 2, it is in both Zones 2 and 3. Nevertheless, there is no continuity of behaviour for Cases 1 and 2 when the droplets evaporate exactly at the flame front. Unless otherwise stated, the governing equations in Section 2.1 are applicable for both cases, but their respective boundary and jump conditions will be presented separately in Section 2.2.

### 2.1. Governing equations

Similar to previous theoretical studies (Belyakov et al., 2018; Han and Chen, 2016, 2015; Blouquin and Joulin, 1998), the liquid droplets in the gas mixture are assumed to be dilute, and therefore the interactions among them are negligible. Also, since the droplet diameter investigated here is small, inter-phasic kinetic equilibrium can be assumed and the particles have the same ve-

locities as gas phase. These simplifications were also used in previous analytical studies of gas-droplet reaction systems (Greenberg, 2007; Greenberg et al., 1996). Meanwhile, in pre-vaporization zone as presented in Fig. 1, thermal equilibrium between droplets and fresh pre-mixture is assumed, and hence they have the same temperatures (Belyakov et al., 2018; Han and Chen, 2016, 2015). The vaporization front is assumed to critically reach the boiling point and therefore evaporation is initiated. Behind this front, the droplet temperature maintains the boiling point and evaporation continues (Belyakov et al., 2018; Han and Chen, 2016, 2015). In addition, the droplet is assumed to be spherical and monodispersed. Note that, in this work, the possible droplet-induced flame front instability and the resultant variations of flame properties are not considered, which is typically caused by the full coupling between the gas and droplet phases.

Eulerian descriptions are adopted for the droplet phase (Crowe et al., 2011), in which case the droplet phase can be treated as an inter-penetrating medium. The Eulerian equation for droplet mass loading  $Y_d$  ( $\equiv \frac{\tilde{N}_d \tilde{m}_d}{\tilde{\rho}_{g0}}$ ) can be derived from single droplet mass equation for  $\tilde{m}_d$  and reads (Hayashi and Kumagai, 1975)

$$\frac{\partial}{\partial \tilde{t}} \left( \frac{\tilde{N}_d \tilde{m}_d}{\tilde{\rho}_{g0}} \right) = \frac{\partial Y_d}{\partial \tilde{t}} = - \frac{\tilde{N}_d \tilde{\omega}_v}{\tilde{\rho}_{g0} \tilde{q}_v}. \quad (1)$$

Here  $\tilde{t}$  is time,  $\tilde{q}_v$  is the latent heat of vaporization per unit mass of water droplet,  $\tilde{N}_d$  is the droplet number density in the unit of volume and  $\tilde{\rho}_{g0}$  is gas density of the fresh mixture.  $\tilde{\omega}_v$  is the droplet evaporation rate and is modelled as (Hayashi and Kumagai, 1975)

$$\tilde{\omega}_v = \tilde{s}_d \frac{\tilde{\lambda}_g Nu}{\tilde{d}} (\tilde{T} - \tilde{T}_v), \quad (2)$$

in which  $\tilde{s}_d = \pi \tilde{d}^2$  is droplet surface area,  $\tilde{\lambda}_g$  is the gas heat conductivity,  $Nu$  is the Nusselt number,  $\tilde{T}$  is the gas temperature,  $\tilde{T}_v$  is the water boiling point, and  $\tilde{d}$  is the droplet diameter.

For gas phase, we adopt the well-known diffusive-thermal model (Joulin and Clavin, 1979), according to which the density, thermal and transport properties are assumed to be constant. The validity of the constant thermal property assumption has been confirmed in the previous detailed numerical simulations of gaseous propagating spherical flames (Chen and Ju, 2007; Li et al., 2018; Zhang et al., 2013a; Zhang and Chen, 2011). Furthermore,

it is assumed that the liquid droplets are dilute and their mass concentration is sufficiently small so that the transport properties are not affected by their presence (Belyakov et al., 2018; Greenberg, 2007; Han and Chen, 2015). Hence, the gas motion induced by thermal-expansion and droplet evaporation can be neglected. These simplifications were also used in previous analytical studies of both gaseous flames and two-phase flames with dispersed liquid droplets (Chen et al., 2011, 2009; Chen and Ju, 2007; Han and Chen, 2016, 2015; He, 2000; Zhang et al., 2013b, 2013a; Zhang and Chen, 2011) and reasonable results are obtained for predicting the general features of spherical flames. As such, the governing equations for temperature and fuel mass fraction of gas phase respectively are

$$\tilde{\rho}_g \tilde{C}_p \frac{\partial \tilde{T}}{\partial \tilde{t}} = \frac{1}{\tilde{r}^2} \frac{\partial}{\partial \tilde{r}} \left( \tilde{r}^2 \tilde{\lambda}_g \frac{\partial \tilde{T}}{\partial \tilde{r}} \right) + \tilde{q}_c \tilde{\omega}_c - \tilde{q}_v \tilde{\omega}_v, \quad (3)$$

$$\tilde{\rho}_g \frac{\partial \tilde{Y}}{\partial \tilde{t}} = \frac{1}{\tilde{r}^2} \frac{\partial}{\partial \tilde{r}} \left( \tilde{r}^2 \tilde{\rho}_g \tilde{D} \frac{\partial \tilde{Y}}{\partial \tilde{r}} \right) - \tilde{\omega}_c, \quad (4)$$

where  $\tilde{r}$  is the radius, and  $\tilde{Y}$  is the fuel mass fraction.  $\tilde{\rho}_g$ ,  $\tilde{C}_p$  and  $\tilde{D}$  are the density, heat capacity and molecular diffusivity of the gaseous fuel, respectively.  $\tilde{q}_c$  is chemical reaction heat release per unit mass of fuel.  $\tilde{\omega}_c$  is the reaction rate for one-step irreversible reaction and is calculated as

$$\tilde{\omega}_c = \tilde{\rho}_g \tilde{A} \tilde{Y} \exp(-\tilde{E}/\tilde{R}^0 \tilde{T}), \quad (5)$$

where  $\tilde{A}$  is the pre-exponential factor of Arrhenius law,  $\tilde{E}$  is the activation energy, and  $\tilde{R}^0$  is the universal gas constant. Besides, radiation heat transfer is not included in this work.

We introduce the following non-dimensional variables

$$U = \frac{\tilde{u}}{\tilde{u}_b}, r = \frac{\tilde{r}}{\tilde{l}_{th}}, t = \frac{\tilde{t}}{\tilde{l}_{th} \tilde{u}_b}, Y = \frac{\tilde{Y}}{\tilde{Y}_0}, T = \frac{\tilde{T} - \tilde{T}_0}{\tilde{T}_b}. \quad (6)$$

Here  $\tilde{T}_0$  and  $\tilde{Y}_0$  denote the temperature and fuel mass fraction in the fresh mixture, respectively.  $\tilde{u}_b$ ,  $\tilde{T}_b = \tilde{q}_c \tilde{Y}_0 / \tilde{C}_p$ ,  $\tilde{l}_{th} = \tilde{D}_{th} / \tilde{u}_b$  are the laminar flame speed, flame temperature and flame thickness of an adiabatic planar flame without water addition, respectively.  $\tilde{D}_{th} = \tilde{\lambda}_g / (\tilde{\rho}_g \tilde{C}_p)$  is the gas thermal diffusivity.

As shown in the previous theoretical analysis for both gaseous flames and two-phase flames with dispersed liquid droplets (Chen et al., 2011, 2009; Chen and Ju, 2007; Han and Chen, 2016, 2015; He, 2000; Zhang et al., 2013b, 2013a; Zhang and Chen, 2011), it is reasonable to adopt the quasi-steady state assumption in the moving coordinate system attached to the propagating flame front  $R_f(t)$ , i.e.  $\eta = r - R_f(t)$ . The validation of this assumption has been demonstrated by transient numerical simulations for gaseous spherical flames without droplets (Chen and Ju, 2007; He, 2000; Li et al., 2018; Zhang and Chen, 2011), in which the unsteady effects are found to have a generally negligible influence in light of the overall balance between diffusion, reaction and convection processes in stably propagating spherical flames. Particularly, when the flame radius is small (e.g. flame kernel solution), as discussed by Chen and Ju (Chen and Ju, 2007), there are only small quantitative differences between the flame propagation speed (versus radius) from the theoretical analysis and transient computations. Some key quantities for flame development, e.g. critical radius and minimum ignition energy, are marginally affected. Hence, this assumption is also valid for the early stage of flame evolutions. Due to relatively dilute water droplet concentration and the chemically inert characteristics, the influences of water droplets on flame zone thickness are small and therefore gaseous combustion still dominates in the studied problem (Belyakov et al., 2018; Han and Chen, 2015). In addition, due to the kinetic equilibrium between two phases, the droplets approximately follow the motion of the gas

phase. Therefore, the quasi-steady state assumption in  $\eta$  coordinate system will be adopted for both gas and droplet equations in the present analysis. The non-dimensional form of the gas and droplet equations, i.e. Eqs. (1), (3) and (4), under the quasi-steady state assumption ( $\partial/\partial t = 0$ ), reads

$$-U \frac{dT}{d\eta} = \frac{1}{(\eta + R_f)^2} \frac{d}{d\eta} \left[ (\eta + R_f)^2 \frac{dT}{d\eta} \right] + \omega_c - \omega_v, \quad (7)$$

$$-U \frac{dY}{d\eta} = Le^{-1} \frac{1}{(\eta + R_f)^2} \frac{d}{d\eta} \left[ (\eta + R_f)^2 \frac{dY}{d\eta} \right] - \omega_c, \quad (8)$$

$$-U \frac{dY_d}{d\eta} = -\frac{\omega_v}{q_v}, \quad (9)$$

where  $U = dR_f(t)/dt$  is the non-dimensional flame propagating speed and  $Le = \tilde{D}_{th} / \tilde{D}$  is the Lewis number. The normalized latent heat of vaporization is  $q_v = \tilde{q}_v / (\tilde{C}_p \tilde{T}_b)$ , and the chemical reaction is  $\omega_c = \tilde{l}_{th} \tilde{\omega}_c / (\tilde{\rho}_g \tilde{u}_b \tilde{Y}_0)$ . Additionally, the non-dimensional droplet evaporation rate  $\omega_v$  is

$$\omega_v = \Omega(T - T_v). \quad (10)$$

Here  $T_v$  is the non-dimensional boiling temperature. The heat exchange coefficient  $\Omega$  in Eq. (10) is

$$\Omega = \pi \tilde{N}_d \text{Nu} \tilde{d}_{th}^2 \tilde{u}_b^{-2}. \quad (11)$$

As shown in Eq. (11), the non-dimensional parameter  $\Omega$  essentially is a lumped parameter affected by both gas and droplet properties. For the latter, it includes droplet diameter  $\tilde{d}$  and number density  $\tilde{N}_d$ . It should be highlighted that for Case 1, as shown in Fig. 1a, Eq. (9) and the evaporation rate term  $\omega_v$  in Eq. (7) are only included in pre-flame zone. However, for Case 2 in Fig. 1b, they are considered in both pre- and post-flame zones.

## 2.2. Jump and boundary conditions

### 2.2.1. Droplet evaporation in pre-flame zone only (Case 1)

The non-dimensional boundary conditions for both gas phase ( $T$  and  $Y$ ) and droplet phase ( $Y_d$ ) equations at the spherical centre ( $\eta = -R_f$ ) and in the fresh mixture ( $\eta \rightarrow \infty$ ) are

$$\eta = -R_f : \quad (\eta + R_f)^2 \frac{dT}{d\eta} = -Q, \quad \frac{dY}{d\eta} = 0, \quad Y_d = 0. \quad (12)$$

$$\eta \rightarrow \infty : \quad T = 0, \quad Y = 1, \quad Y_d = \delta. \quad (13)$$

Here  $\delta$  is the initial mass loading of the water droplets in the fresh mixture, and  $Q$  is the normalized ignition energy. The steady-state deposition of the ignition energy is provided as an energy flux at the centre, which is also adopted by the previous theoretical studies about ignition of spherical flames (Chen and Ju, 2007; Han and Chen, 2015; He, 2000; Zhang et al., 2013a; Zhang and Chen, 2011). As demonstrated by the transient calculations of spherical flames in (Chen et al., 2011, 2009; Chen and Ju, 2007; He, 2000; Zhang et al., 2013b, 2013a; Zhang and Chen, 2011), this simplification is adequate to gain qualitative understanding of spherical flame initiation and propagation, which will be discussed in Section 4.2.

At the vaporization front,  $\eta = \eta_v = R_v - R_f$ , the gas temperature  $T$ , fuel mass fraction  $Y$  and droplet mass loading  $Y_d$  satisfy the following jump conditions (Belyakov et al., 2018; Han and Chen, 2016, 2015)

$$T = T_v, [Y] = [T] = \left[ \frac{dY}{d\eta} \right] = \left[ \frac{dT}{d\eta} \right] = 0, [Y_d] = 0. \quad (14)$$

In the limit of large activation energy, chemical reactions in gas phase are confined at an infinitesimally thin flame sheet (i.e.  $\eta = 0$ ) (Chen and Ju, 2007; Joulin and Clavin, 1979). The corresponding jump conditions at  $\eta = 0$  are

$$T = T_f, Y = 0, Y_d = 0, -\left[\frac{dT}{d\eta}\right] = Le^{-1}\left[\frac{dY}{d\eta}\right] = [\sigma + (1 - \sigma)T_f]^2 \exp\left[\frac{Z}{2}\left(\frac{T_f - 1}{\sigma + (1 - \sigma)T_f}\right)\right], \quad (15)$$

where  $T_f$  is the flame temperature,  $\sigma$  is the thermal expansion ratio and  $Z$  is the Zel'dovich number. The square brackets, i.e.  $[f] = f(\eta^+) - f(\eta^-)$ , denote the difference between the variables at two sides of the vaporization front ( $\eta = \eta_v$ ) or flame sheet ( $\eta = 0$ ).

2.2.2. Droplet evaporation in pre- and post-flame zones (Case 2)

The corresponding boundary conditions at the spherical centre ( $\eta = -R_f$ ) and in the fresh mixture ( $\eta \rightarrow \infty$ ) are the same as Case 1, i.e. Eqs. (12) and (13), except that  $dT/d\eta = 0$  should be used, instead of  $(\eta + R_f)^2 dT/d\eta = -Q$ . The reason is that the energy boundary condition may cause the present algebraic system unsolvable when the water droplet is fully vaporized critically at the spherical centre. As a future topic, ignition of droplet-laden spherical flames in Case 2 will be investigated through relaxing the above assumption about the front of vaporization completion, as done by Belyakov et al. in (Belyakov et al., 2018) for planar flames.

$$\mathfrak{R}_1 = \frac{G(-k \cdot (R_f + \eta_v), \frac{U}{k}, -\frac{U}{k}) \cdot F(k(R_f + \eta), \frac{U}{k}, -\frac{U}{k}) - F(k(R_f + \eta_v), \frac{U}{k}, -\frac{U}{k}) \cdot G(-k \cdot (R_f + \eta), \frac{U}{k}, -\frac{U}{k})}{G(-k \cdot (R_f + \eta_v), \frac{U}{k}, -\frac{U}{k}) \cdot F(k(R_f + \eta_v), 1 + \frac{U}{k}, -\frac{U}{k}) + F(k(R_f + \eta_v), \frac{U}{k}, -\frac{U}{k}) \cdot G(-k \cdot (R_f + \eta_v), 1 + \frac{U}{k}, -\frac{U}{k})}$$

The jump conditions at the vaporization front are the same as those in Case 1, i.e. Eq. (14). In addition, the jump conditions at the thin flame sheet are the same as in Case 1, i.e. Eq. (15), except that  $[Y_d] = 0$  (i.e. continuous distribution of droplet across the flame front) should be used, instead of  $Y_d = 0$ .

3. Theoretical analysis

Eqs. (7)–(9) with proper jump and boundary conditions for Cases 1 and 2 are solved analytically in pre-vaporization zone ( $\eta_v \leq \eta < \infty$ , Zone 1 in Fig. 1), pre-flame zone ( $0 \leq \eta < \eta_v$ , Zone 2) and post-flame zone ( $-R_f \leq \eta < 0$ , Zone 3). The reader is reminded here that the effects of various distributions of droplet evaporation on spherical flame initiation and propagation (i.e. Case 1 and Case 2) are investigated in the current analysis. As such, both of their solutions will be presented below.

3.1. Droplet evaporation in pre-flame zone only (Case 1)

$$\mathfrak{R}_2 = \frac{G(-k \cdot (R_f + \eta_v), \frac{U}{k}, -\frac{U}{k}) \cdot F(kR_f, \frac{U}{k}, -\frac{U}{k}) - F(k(R_f + \eta_v), \frac{U}{k}, -\frac{U}{k}) \cdot G(-kR_f, \frac{U}{k}, -\frac{U}{k})}{G(-k \cdot (R_f + \eta_v), \frac{U}{k}, -\frac{U}{k}) \cdot F(k(R_f + \eta_v), 1 + \frac{U}{k}, -\frac{U}{k}) + F(k(R_f + \eta_v), \frac{U}{k}, -\frac{U}{k}) \cdot G(-k \cdot (R_f + \eta_v), 1 + \frac{U}{k}, -\frac{U}{k})}$$

where

$$\mathfrak{R}_3 = \frac{G(-k \cdot (R_f + \eta_v), \frac{U}{k}, -\frac{U}{k}) \cdot F(kR_f, 1 + \frac{U}{k}, -\frac{U}{k}) + F(k \cdot (R_f + \eta_v), \frac{U}{k}, -\frac{U}{k}) \cdot G(-kR_f, 1 + \frac{U}{k}, -\frac{U}{k})}{G(-k \cdot (R_f + \eta_v), \frac{U}{k}, -\frac{U}{k}) \cdot F(k \cdot (R_f + \eta_v), 1 + \frac{U}{k}, -\frac{U}{k}) + F(k \cdot (R_f + \eta_v), \frac{U}{k}, -\frac{U}{k}) \cdot G(-k \cdot (R_f + \eta_v), 1 + \frac{U}{k}, -\frac{U}{k})}$$

3.2. Droplet evaporation in pre- and post-flame zones (Case 2)

(1) Distributions of temperature, fuel mass fraction and droplet mass loading

The solutions for temperature, fuel mass fraction and droplet mass loading in Zones 1–3 are

$$T = \begin{cases} T_v \frac{I_1(\eta, U)}{I_1(\eta_v, U)}, & \text{if } \eta_v \leq \eta < \infty \\ T_v - \frac{T_v(\eta_v + R_f)^{-2} e^{0.5(U+k)(\eta_v-\eta)-U(\eta_v+R_f)} \Gamma(2 + \frac{U}{k})}{I_1(\eta_v, U)(k+U) \Gamma(1 + \frac{U}{k})} \mathfrak{R}_1, & \text{if } 0 \leq \eta < \eta_v, \\ T_f + Q[I_1(0, U) - I_1(\eta, U)], & \text{if } -R_f \leq \eta < 0 \end{cases} \quad (16)$$

$$Y = \begin{cases} 1 - \frac{I_1(\eta, LeU)}{I_1(0, LeU)}, & \text{if } 0 \leq \eta < \infty \\ 0, & \text{if } -R_f \leq \eta < 0 \end{cases}, \quad (17)$$

$$Y_d = \begin{cases} \delta, & \text{if } \eta_v \leq \eta < \infty \\ \delta \frac{\int_{-R_f}^{\eta} (T_2 - T_v) d\xi}{\int_{-R_f}^{\eta_v} (T_2 - T_v) d\xi}, & \text{if } 0 \leq \eta < \eta_v, \\ 0, & \text{if } -R_f \leq \eta < 0 \end{cases} \quad (18)$$

where  $k = \sqrt{4\Omega + U^2}$ ,  $I_1(x, y) = e^{-yR_f} \int_x^{+\infty} (\xi + R_f)^{-2} e^{-y\xi} d\xi$ ,  $\Gamma(a) = \int_0^{\infty} t^{a-1} e^{-t} dt$ ,  $F(a, b, c) = \int_0^1 t^b e^{at} (1-t)^c dt$ ,  $G(a, b, c) = \int_0^{\infty} t^b e^{at} (1+t)^c dt$ , and

(2) Correlations for propagating spherical flames with droplet evaporation

Based on the jump conditions in Eq. (15), one obtains the following algebraic system for the correlations between flame temperature  $T_f$ , flame propagating speed  $U$ , flame radius  $R_f$ , and vaporization front  $\eta_v$ :

$$T_f = T_v - \frac{T_v(\eta_v + R_f)^{-2} e^{0.5(U+k)\eta_v-U(\eta_v+R_f)} \Gamma(2 + \frac{U}{k})}{I_1(\eta_v, U)(k+U) \Gamma(1 + \frac{U}{k})} \mathfrak{R}_2, \quad (19)$$

$$\begin{aligned} & -QR_f^{-2} e^{-UR_f} + 0.5(k+U)(T_f - T_v) \\ & + \frac{T_v(\eta_v + R_f)^{-2} e^{0.5(U+k)\eta_v-U(\eta_v+R_f)}}{I_1(\eta_v, U)} \\ \mathfrak{R}_3 = & \frac{1}{Le} \frac{R_f^{-2} e^{-LeUR_f}}{I_1(0, LeU)} = [\sigma + (1 - \sigma)T_f]^2 \exp\left[\frac{Z}{2} \frac{T_f - 1}{\sigma + (1 - \sigma)T_f}\right], \end{aligned} \quad (20)$$

where

3.2. Droplet evaporation in pre- and post-flame zones (Case 2)

(1) Distributions of temperature, fuel mass fraction and droplet mass loading

(1) Distributions of temperature, fuel mass fraction and droplet mass loading

The solutions for temperature, fuel mass fraction and droplet mass loading in Zones 1–3 are

$$T = \begin{cases} T_v \frac{I_1(\eta, U)}{I_1(\eta_v, U)}, & \text{if } \eta_v \leq \eta < \infty \\ T_v - \frac{T_v(\eta_v + R_f)^{-2} e^{0.5(U+k)(\eta_v - \eta) - U(\eta_v + R_f)} \Gamma(2 + \frac{U}{k})}{I_1(\eta_v, U)(k+U) \Gamma(1 + \frac{U}{k})} \mathfrak{M}_1, & \text{if } 0 \leq \eta < \eta_v \\ T_v + e^{-0.5(U+k)\eta} (T_f - T_v) \frac{F(k(R_f + \eta), \frac{U}{k}, -\frac{U}{k})}{F(kR_f, \frac{U}{k}, -\frac{U}{k})}, & \text{if } -R_f \leq \eta < 0 \end{cases} \quad (21)$$

$$Y = \begin{cases} 1 - \frac{I_1(\eta, LeU)}{I_1(0, LeU)}, & \text{if } 0 \leq \eta < \infty \\ 0, & \text{if } -R_f \leq \eta < 0 \end{cases} \quad (22)$$

$$Y_d = \begin{cases} \delta, & \text{if } \eta_v \leq \eta < \infty \\ \delta \frac{\int_{-R_f}^0 (T_3 - T_v) d\xi + \int_0^{\eta_v} (T_2 - T_v) d\xi}{\int_{-R_f}^0 (T_3 - T_v) d\xi + \int_0^{\eta_v} (T_2 - T_v) d\xi}, & \text{if } 0 \leq \eta < \eta_v \\ \delta \frac{\int_{-R_f}^{\eta} (T_3 - T_v) d\xi}{\int_{-R_f}^0 (T_3 - T_v) d\xi + \int_0^{\eta_v} (T_2 - T_v) d\xi}, & \text{if } -R_f \leq \eta < 0 \end{cases} \quad (23)$$

(2) Correlations for propagating spherical flames with droplet evaporation

The explicit expression of flame temperature for Case 2 is the same as that from Case 1, i.e. Eq. (19), and hence will be not repeated here. By using the jump conditions of Case 2, one can obtain the following algebraic system

$$\frac{\Gamma(1 + \frac{U}{k}) F(kR_f, 1 + \frac{U}{k}, -\frac{U}{k})(k+U)(T_f - T_v)}{\Gamma(2 + \frac{U}{k}) F(kR_f, \frac{U}{k}, -\frac{U}{k})} + \frac{T_v(\eta_v + R_f)^{-2} e^{0.5(U+k)\eta_v - U(\eta_v + R_f)} I_1(\eta_v, U)}{I_1(\eta_v, U)} \mathfrak{M}_3 = \frac{1}{Le} \frac{R_f^{-2} e^{-LeUR_f}}{I_1(0, LeU)} = [\sigma + (1 - \sigma)T_f]^2 \exp\left[\frac{Z}{2} \frac{T_f - 1}{\sigma + (1 - \sigma)T_f}\right]. \quad (24)$$

Eqs. (19) and (20), as well as Eqs. (19) and (24), describe the correlations between flame propagation speed  $U$ , radius  $R_f$ , temperature  $T_f$ , and vaporization front  $\eta_v$  when the droplet laden spherical flames are initiated and propagate outwardly in Case 1 and Case 2, respectively. Therefore, the influences of the different distributions of water droplets from Case 1 and Case 2 can be compared. Various parameters are included in the foregoing equations, including Lewis number ( $Le$ ), heat exchange coefficient ( $\Omega$ ), and ignition energy ( $Q$ ). Therefore, their effects on initiation and propagation of spherical flames can be discussed through numerically solving Eqs. (19), (20) and (24).

The current models of Case 1 and Case 2 can recover the correlation for droplet-laden spherical flames without central energy deposition ( $Q=0$ ) (Chen and Ju, 2007) in the limit of  $\delta \rightarrow 0$ . For Case 1 in which the flame ignition is taken into consideration, its model can be reduced to the results about ignition ( $Q > 0$ ) of droplet-free spherical flames also derived by Chen and Ju (Chen and Ju, 2007). In addition, when the flame radius is infinite ( $R_f \rightarrow +\infty$ ) which corresponds to propagating planar flames, the current models of both cases can give the consistent results for planar flames with the same initial droplet distributions (Belyakov et al., 2018). As such, the current theoretical model can be successfully simplified into different situations under various limits.

#### 4. Results and discussion

The constants used in the following analysis include (Belyakov et al., 2018; Chen and Ju, 2007): Zel'dovich number  $Z=10$ , thermal expansion ratio  $\sigma=0.15$ , normalized boiling point of water  $T_v = 0.222$ , normalized latent heat of water evaporation  $q_v = 1.256$ ,

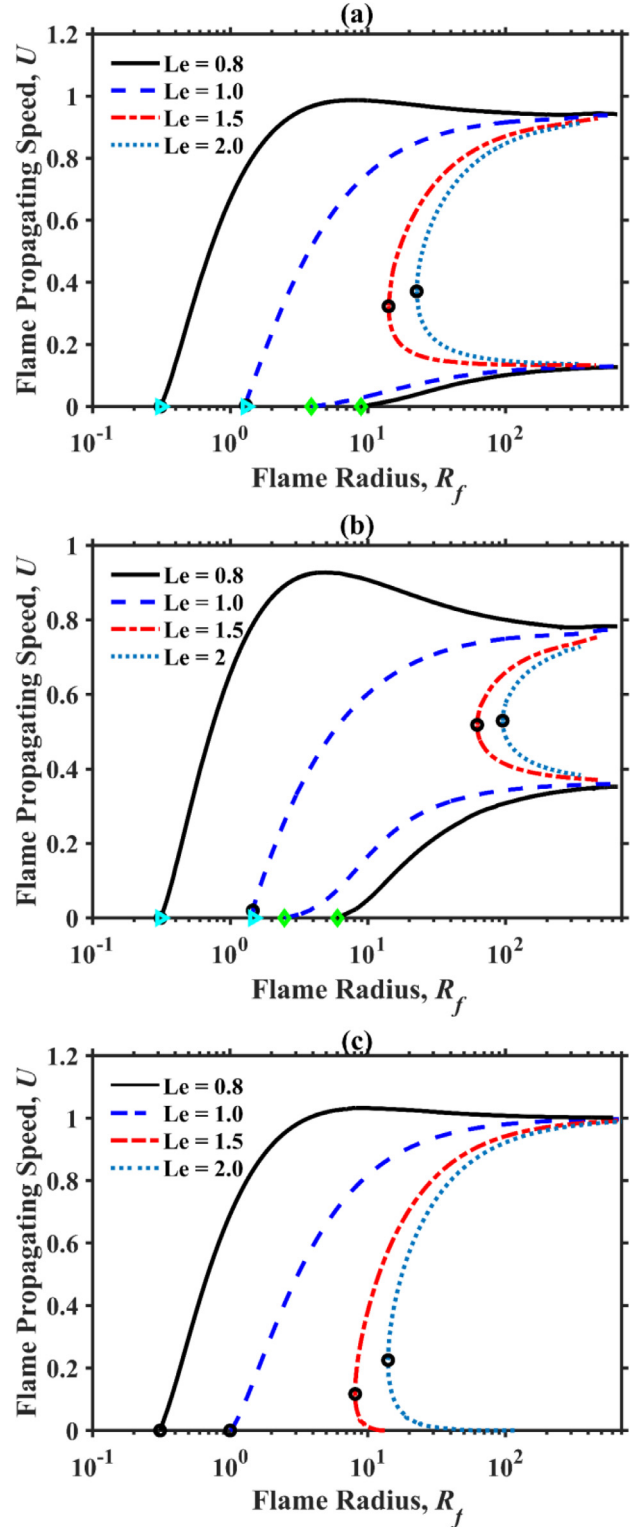
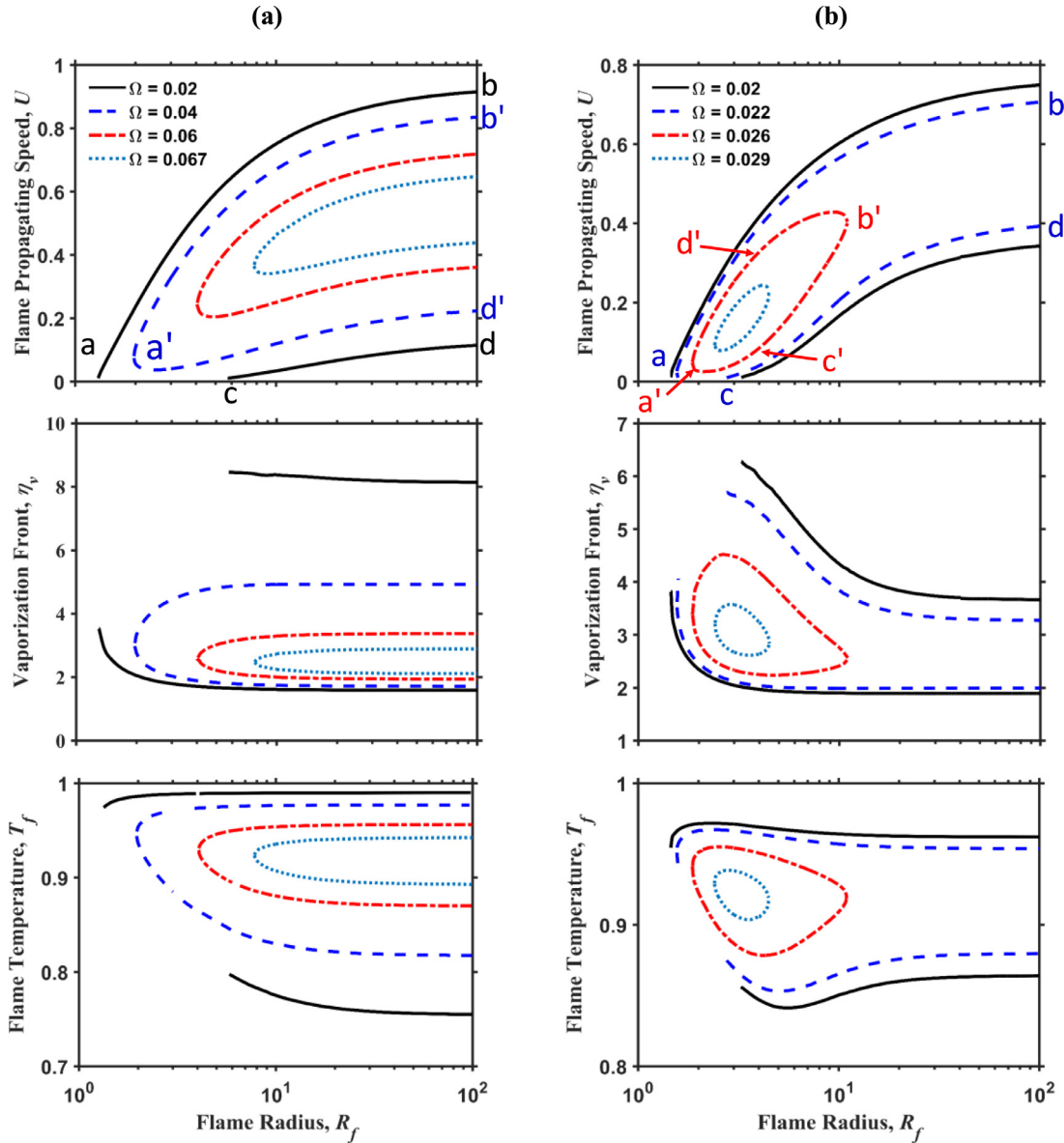


Fig. 2. Flame propagating speed as a function of flame radius for different Lewis numbers at  $Q=0$  with and without droplets: (a) Case 1 at  $\Omega=0.02$ ; (b) Case 2 at  $\Omega=0.02$ ; (c)  $\Omega=0$ . The critical flame radii  $R_c$ , left and right flame ball radii ( $R_L^*$  and  $R_R^*$ ) are denoted by circles, triangles and diamonds, respectively.



**Fig. 3.** Flame propagation speed, vaporization front and flame temperature as functions of flame radius for different heat exchange coefficients at  $Le = 1.0$  in (a) Case 1 and (b) Case 2. The symbols  $abcd$  and  $a'b'c'd'$  are used to identify the different regimes for analysis in Figs. 7 and 8.

initial droplet mass loading  $\delta = 0.2$ . Note that these values of  $T_v$  and  $q_v$  correspond to the properties of liquid water at atmospheric pressure (Belyakov et al., 2018).

#### 4.1. Spherical flame propagation and extinction

Fig. 2a–c show the flame propagation speed as a function of flame radius at  $Q = 0$  with and without droplets. The influences of Lewis numbers on spherical flame propagation are examined. The solutions on the horizontal axis with  $U = 0$  denote stationary flame ball solutions (left  $R_2^-$  marked by triangles and right  $R_2^+$  marked by diamonds). It is noted that there exists a critical flame radius ( $R_c$ , marked by open circles), beyond which propagating spherical flames can be achieved. Fig. 2a shows that in Case 1, for  $Le = 0.8$ , there are two branches (upper stable flame and lower unstable flame), and  $R_c$  is equal to  $R_2^-$ . Along the stable flame branch, the flame propagation speed first increases, then slightly decreases and finally tends to be approximately 0.95 at large  $R_f$  ( $U = 1$  for adia-

batic gaseous flames (Chen and Ju, 2007)). The increase is caused by the transition from the flame balls dominated by diffusion to the outwardly propagating spherical flames dominated jointly by convection and diffusion. The decrease is due to the preferential effects of flame stretch (i.e.  $K \equiv 2U/R_f$  for spherical flames) and the small Lewis number (Law, 2006; Chen and Ju, 2007; Zhang et al., 2013a; Zhang and Chen, 2011). When  $Le = 1.0$ , there are still two branches, but the above mentioned non-monotonic behaviour for the upper branch does not exist. When  $Le$  is increased to 1.5 and 2.0, C-shaped solutions are observable. In these scenarios,  $R_c$  is at the turning point, which demarcates the upper stable branch and lower unstable branch. These characteristics are also observed in previous theoretical analysis for gaseous spherical premixed flames (Chen et al., 2011, 2009; Chen and Ju, 2007; He, 2000; Zhang et al., 2013b, 2013a; Zhang and Chen, 2011).

Through comparing Fig. 2a and b, one can find that Case 1 and Case 2 have qualitatively similar solution distributions in the  $U$ - $R_f$  plane. Nevertheless, in Case 2, the flame propagation speed  $U$

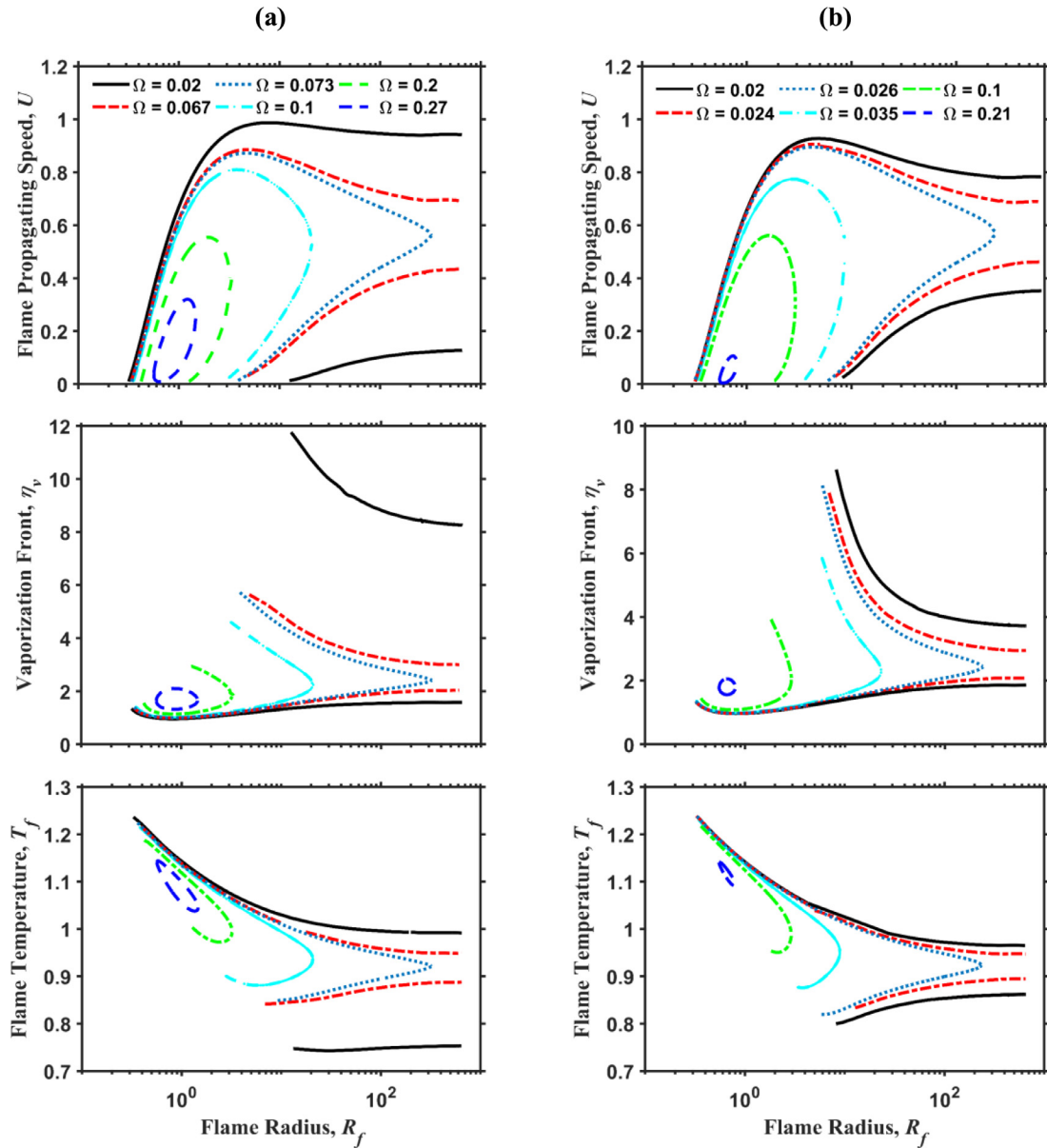


**Fig. 4.** Flame propagation speed, vaporization front and flame temperature as functions of flame radius for different heat exchange coefficients at  $Le=0.8$  in (a) Case 1 and (b) Case 2.

is consistently lower than that in Case 1 with the same  $Le$ . This is because in Case 2 the droplets are dispersed in the entire domain and the gas phase heat loss due to water droplet evaporation are stronger. Also, for the critical flame radii  $R_c$  which indicate the initiation of the stable flame branches, the influence of different droplet distributions in two cases on  $R_c$  becomes more pronounced with increased  $Le$ . This is particularly true for large  $Le$  (say 1.5 and 2). In fact, when the water droplets are presented in the gas mixture, the heat loss from their evaporation competes with the Lewis number effects. When the latter enhances the flame, the flame can be sustained at the similar critical radii in both Cases. Nevertheless, when it weakens the flame (e.g.  $Le = 1.5$  and 2), the droplet distributions in Case 2 render the spherical flames be sustained at a larger radius and therefore a weaker stretch rate than in Case 1. Moreover, through comparing results with (Fig. 2a and b) and without droplets (Fig. 2c), there is only one branch for pure gaseous flames and flame speed eventually reaches the planar flame speed ( $U=1$ ) at a large  $R_f$ . Also, the critical flame radius  $R_c$  without droplets is smaller than that with droplets at a fixed

$Le$ . The same trend of results in Fig. 2c was observed in previous theoretical analysis for gaseous spherical premixed flames (Chen et al., 2011, 2009; Chen and Ju, 2007; He, 2000; Zhang et al., 2013b, 2013a; Zhang and Chen, 2011), which also qualitatively confirms the results obtained from our theoretical model.

Fig. 3a and b show flame propagation speed  $U$ , vaporization front  $\eta_v$  and flame temperature  $T_f$  as functions of flame radius  $R_f$  at  $Le = 1$  in Case 1 and Case 2, respectively. The effects of various heat exchange coefficients  $\Omega$  are discussed. In Fig. 3a, when  $\Omega = 0.02$ , dual flame ball solutions exist. As  $\Omega$  increases, the flame ball solutions do not exist, the separate stable and unstable branches become a C-shaped curve and the critical flame radius  $R_c$  at the turning point increases. When  $\Omega > 0.067$ , the C-shaped curve cannot be found and this droplet-laden mixture becomes not flammable due to the heat loss from droplet evaporation. This indicates that the spherical flame reaches its flammability limit at relatively large radius (with weak stretch). The propagation speed at extinction is about  $U \approx 0.55$ . This value is consistent with the prediction from the freely propagation planar

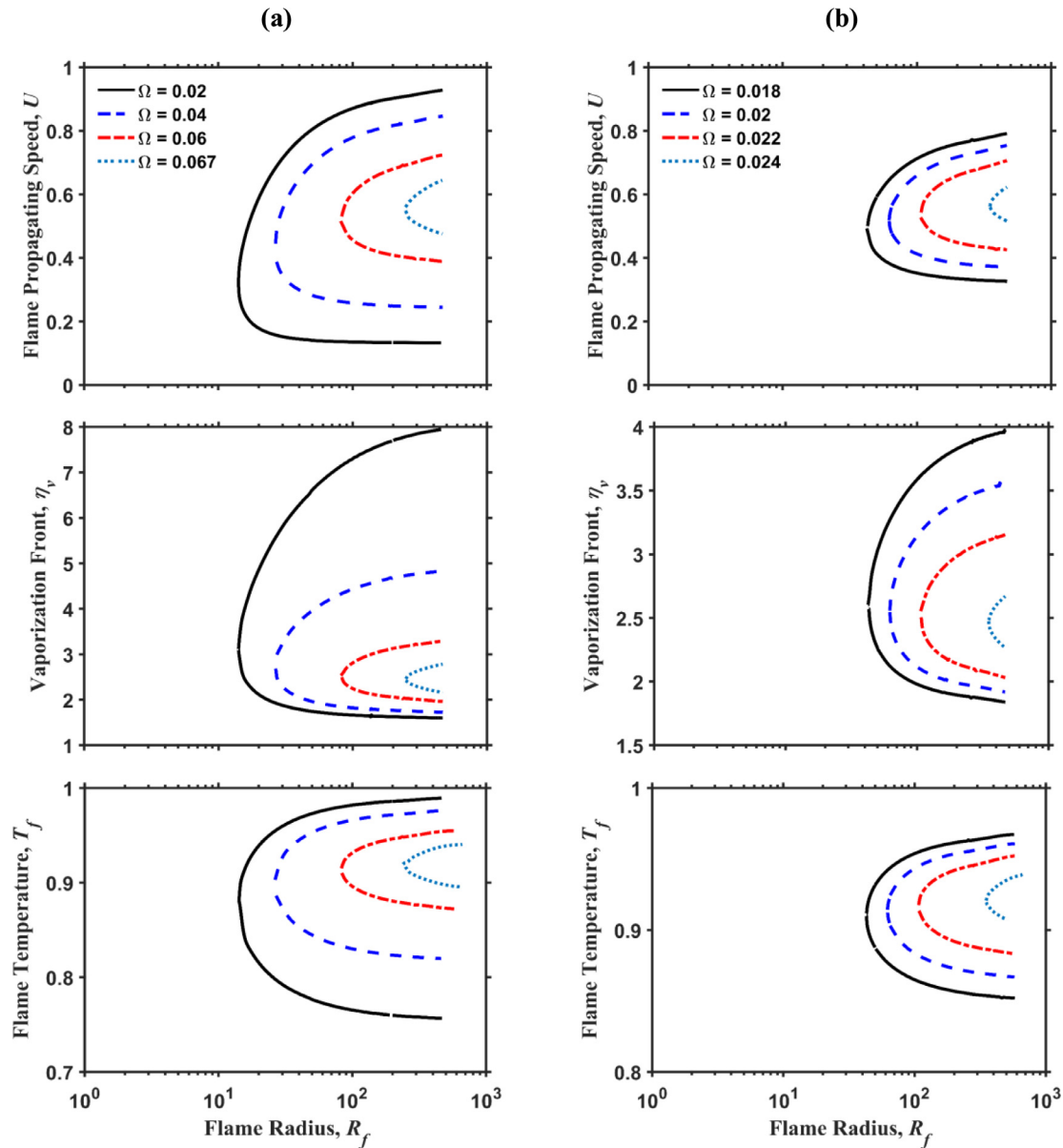


Fig. 5. Flame propagation speed, vaporization front and flame temperature as functions of flame radius for different heat exchange coefficients at  $Le = 1.5$  in (a) Case 1 and (b) Case 2.

flames (Belyakov et al., 2018), close to the results (50%–60% of the adiabatic burning velocity) obtained by Blouquin and Joulin (Blouquin and Joulin, 1998).

In Case 1, the vaporization front  $\eta_v$  has two branches at  $\Omega = 0.02$ , and these branches evolve into C-shaped curves with increased  $\Omega$ , as presented in Fig. 3(a). The upper stable flame branch corresponds to the lower branch of  $\eta_v$  and upper branch of  $T_f$ . It can be seen that  $\eta_v$  is directly affected by  $T_f$  for a fixed  $\Omega$ . Specifically, the higher  $T_f$  leads to smaller  $\eta_v$ , indicating that it is closer to the flame front  $R_f$ . When the temperature variation is small for propagating spherical flames with large radii,  $\eta_v$  is close to be constant. However,  $\eta_v$  consistently increases with  $\Omega$ , since lower  $T_f$  due to the stronger heat loss from droplet evaporation spatially delays the onset of the vaporization in the pre-flame zone.

Similarly, the effects of heat exchange coefficient  $\Omega$  in Case 2 are demonstrated in Fig. 3b. The qualitatively similar behaviours of  $U$ ,  $T_f$  and  $\eta_v$  with  $R_f$  can be observed at  $\Omega = 0.02$  and 0.022 as in Case 1 from Fig. 3a. However, when  $\Omega$  increases to 0.026 and 0.029, a new flame regime, isolated Self-Extinguishing Flames

(SEF), can be observed at intermediate radii. The extinction at the right turning point of SEF curves may be caused by the simultaneous heat transfer due to droplet evaporation from both Zones 2 and 3. This was also seen from the theoretical analysis by Chen and Ju (Chen and Ju, 2007), where the radiation heat loss in both burned and unburned zones is considered for spherical gaseous flames. For SEFs at  $\Omega = 0.026$  and 0.029,  $\eta_v$  and  $T_f$  vary with  $R_f$  non-monotonically. The flame temperature  $T_f$  first increases and then decreases, whereas  $\eta_v$  has the opposite tendency. The effects of water droplets on the SEFs will be discussed further below through calculating the normalized evaporation heat loss in Fig. 8. Unlike Case 1, when the droplets are present in the whole domain, the flame reaches its flammability limit in the form of the shrinking SEFs at intermediate radii, instead of that for the planar droplet-laden flames (as shown in Fig. 3a). The propagation speed at extinction in Case 2 ( $< 0.2$ ) is much lower than that in Case 1 ( $\sim 0.55$ ). Meanwhile, the heat exchange coefficient corresponding to this flammability limit is much lower in Case 2 (0.029) than that in Case 1 (0.067).

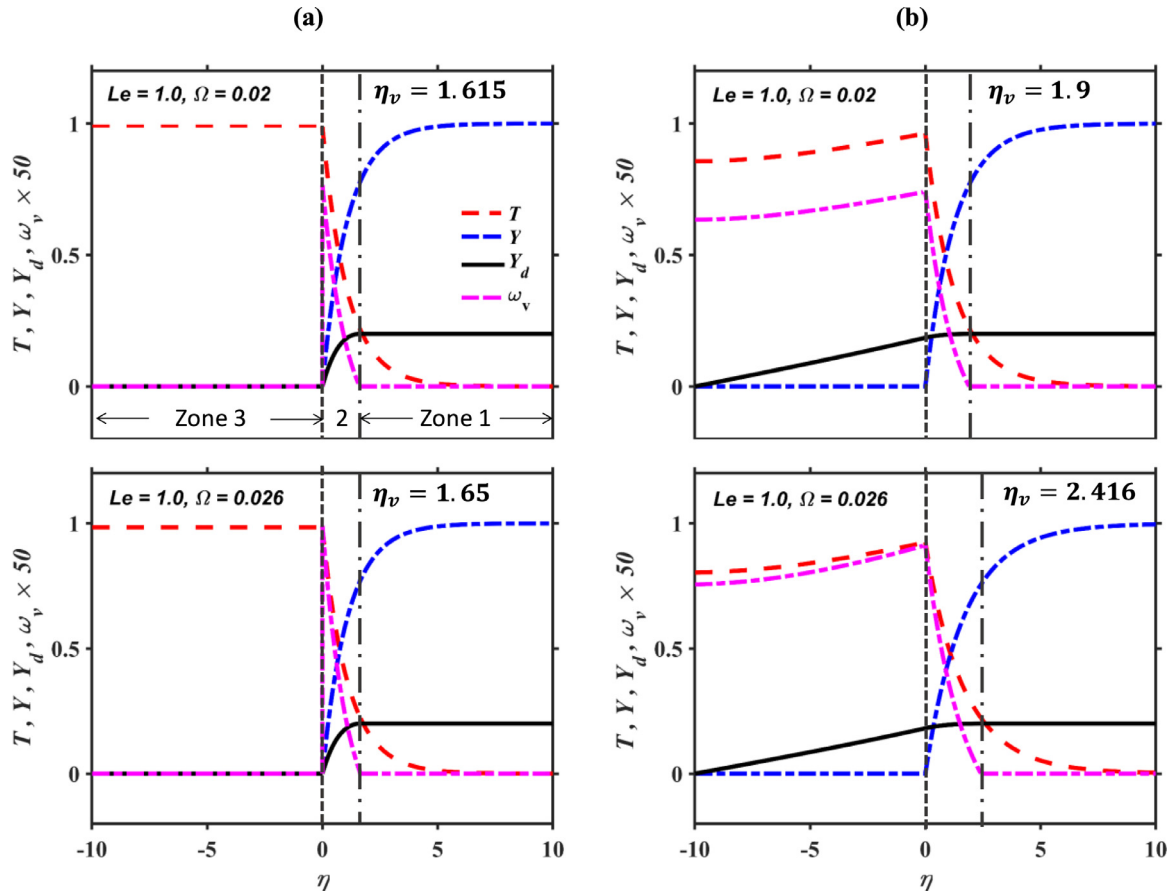


**Fig. 6.** Distributions of temperature, fuel mass fraction, droplet mass loading and evaporation rate for different heat exchange coefficients at  $Le = 1.0$  in (a) Case 1 and (b) Case 2. The spherical centre is at  $\eta = -10$  ( $R_f = 10$ ). Dash lines: flame fronts ( $\eta = 0$ ); Dash-dotted lines: vaporization fronts ( $\eta_v$  indicated).

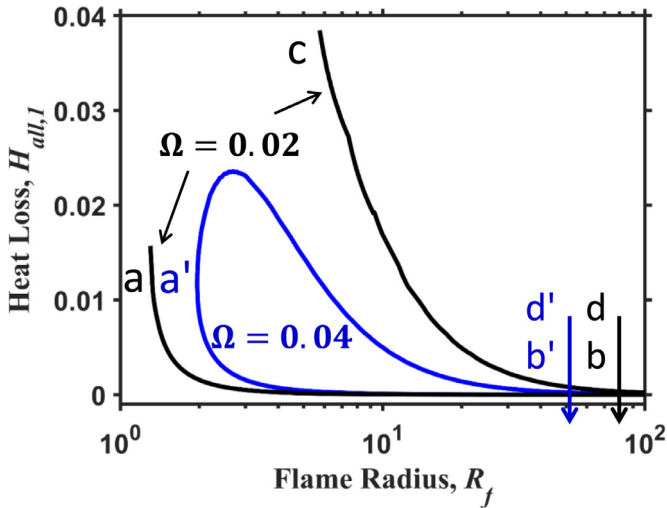


**Fig. 7.** The dependence of normalized evaporation heat loss on flame radius for Case 1 with  $Le = 1$ . The symbols here consistent with those in Fig. 3a.

The combined effects of Lewis number and heat loss due to droplet phase on spherical flame propagation will be further investigated in Fig. 4 ( $Le = 0.8$ ) and Fig. 5 ( $Le = 1.5$ ). Similarly, both Case 1 and Case 2 will be discussed to analyse the effects of different droplet distributions. It is seen in Fig. 4 that when  $Le = 0.8$ , evolutions of  $U$ ,  $T_f$  and  $\eta_v$  with  $R_f$  are qualitatively similar for both cases. Besides the outwardly propagating spherical flames (at small  $\Omega$ ) and SEFs (at large  $\Omega$ ), at intermediate  $\Omega$ , a new regime arises,

i.e. sub-limit SEFs (e.g.  $\Omega = 0.1$  in Case 1 and  $\Omega = 0.035$  in Case 2), along which the flames can be initiated from a flame ball solution but are quenched at a critical radius. The similar bifurcation behaviours are observed in previous studies for radiative spherical flames (Chen and Ju, 2007). At  $Le = 0.8$ , for both cases, the flammability limits are gradually reached with the limiting solutions of SEFs. The critical values for  $\Omega$  for these limits are around 0.27 and 0.21 for Case 1 and Case 2, respectively. One can see that the  $T_f$  is larger than unity when the propagating flames are highly stretched at small and intermediate radii (e.g.  $R_f < 50$ ) for all the considered  $\Omega$ . This indicates that the enhancement effects of the positive stretch rate and small Lewis number dominate the heat loss effects from droplet evaporation. In this scenario,  $\eta_v$  is slightly influenced by  $\Omega$ , as shown in Fig. 4, before the flammability limit is approached.

At  $Le = 1.5$ , no flame balls, sub-limit SEFs and SEFs exist for the two cases, which can be seen from Fig. 5a and b, respectively. Instead,  $U - R_f$  solutions with different  $\Omega$  are characterized as the C-shaped curves with upper stable propagating spherical flames beyond critical flame radii  $R_c$ . The flame can only propagate at relatively large radii, where the weakening effects from positive stretch rate and large Lewis number become comparatively small.  $R_c$  is expected to become larger when the droplet cooling effects are considered, since both effects jointly weaken the spherical flame propagation when  $Le > 1$ . As shown in Fig. 5b, the weakening is stronger when the droplets appear in pre- and post-flame zones. When  $\Omega$  is critically large, the gas-droplet mixture is not flammable. This critical  $\Omega$  in Case 1 is about 0.067, while in Case 2 about 0.024. For  $\eta_v$  and  $T_f$ , they show monotonic decrease and increase with increased flame radius.

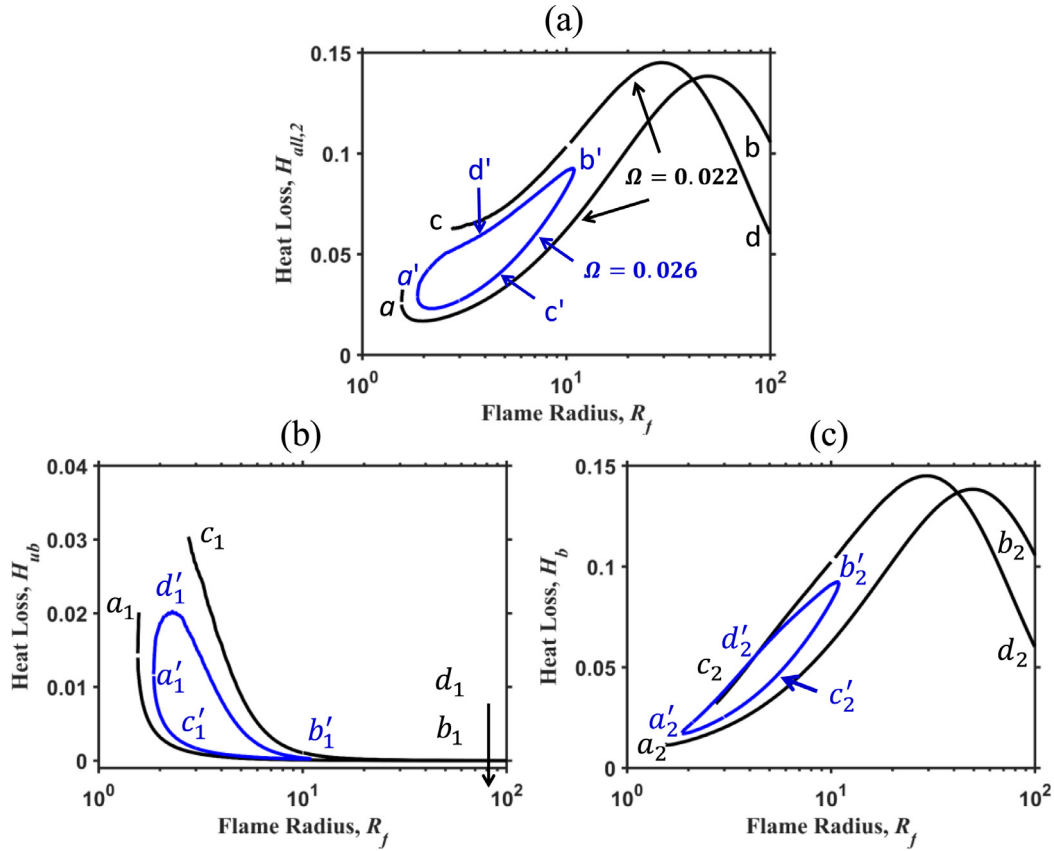


Fig. 8. The dependence of normalized evaporation heat loss on flame radius for Case 2 with  $Le = 1$ : (a)  $H_{all,2}$ , (b)  $H_{ub}$ , and (c)  $H_b$ . The symbols in (a) consistent with those in Fig. 3b.

Fig. 6 shows the spatial distributions of gas temperature, fuel mass fraction, droplet mass loading and evaporation rate for the spherical flames with radius  $R_f = 10$  at  $Le = 1$ . Note that Fig. 6a corresponds to Case 1, in which the droplets are only presented in vaporization zone and pre-flame zone, whereas Fig. 6b shows the results when the droplets are dispersed in the full domain.  $\Omega = 0.02$  and  $0.026$  are considered for comparisons. Three observations can be made based on Fig. 6. Firstly, the evaporation rate  $\omega_v$  in Case 1 is spiky close to the flame front in Zone 2, whereas for Case 2 considerable  $\omega_v$  can be observed in both Zones 2 and 3. As such, in Case 2, the gas temperature gradually decreases towards the spherical centre, which differs from Case 1. In the latter, the temperature in the burned zone is constant. Also, the temperature gradient in Zone 3 also reduces  $T_f$  through heat conduction and therefore flame temperature  $T_f$  in Case 2 is consistently lower than that in Case 1. Secondly, in Case 2, the vaporization front  $\eta_v$  is higher than that in Case 1 with same heat exchange coefficient  $\Omega$ . For instance, when  $\Omega = 0.02$ ,  $\eta_v = 1.9$  in Case 2 higher than  $\eta_v = 1.615$  in Case 1. Since  $\eta_v$  is the critical location where the temperature critically reaches the boiling point and hence the droplet evaporation starts, the above differences of  $\eta_v$  can be justified through comparing the temperature profiles in Zone 1. For Case 2, the lower gas temperature due to combined vaporization in Zones 2 and 3, and the more distributed gas temperature in Zones 1 and 2, which makes the mixture reach the boiling point farther from the flame front and hence larger  $\eta_v$ . This is also observed by Belyakov et al. in their theoretical analysis for planar flames with water mists (Belyakov et al., 2018).

The relation between heat exchange coefficient  $\Omega$  and vaporization front  $\eta_v$  is also shown in Fig. 6. When droplet evaporation occurs only before the flame front as presented in Fig. 6a, the

temperature profiles are only slightly affected by increased  $\Omega$  from 0.02 to 0.026, which results in the small change of  $\eta_v$ . In Case 2, when  $\Omega$  is increased, the flame temperature  $T_f$  and temperature in the burned zone are noticeably reduced, but the temperature before the flame front is slightly increased. This directly leads to bigger locations of onset of droplet evaporation. These findings are consistent with the results in Fig. 3. The relations between  $\Omega$  and  $\eta_v$  are also affected by various Lewis numbers. This is particularly obvious when  $Le > 1$  as shown in Fig. 5: the higher  $\Omega$ , the farther the vaporization front is from the flame.

To gain an insight into how droplet evaporation affects various flame regimes (e.g. SEF), the normalized evaporation heat loss can be calculated in the pre-flame (Zone 2) and post-flame (Zone 3) zones respectively as

$$H_{ub} = \Omega \int_0^{\eta_v} [T_2(\xi) - T_v] \xi^2 d\xi / \left( R_f^2 \frac{dT}{d\eta} \Big|_{0^-} - R_f^2 \frac{dT}{d\eta} \Big|_{0^+} \right), \quad (25)$$

$$H_b = \Omega \int_{-R_f}^0 [T_3(\xi) - T_v] \xi^2 d\xi / \left( R_f^2 \frac{dT}{d\eta} \Big|_{0^-} - R_f^2 \frac{dT}{d\eta} \Big|_{0^+} \right), \quad (26)$$

where  $(R_f^2 \frac{dT}{d\eta} \Big|_{0^-} - R_f^2 \frac{dT}{d\eta} \Big|_{0^+})$  is the total heat release from chemical reaction.  $T_2$  and  $T_3$  denote the temperature distributions in Zone 2 and Zone 3, respectively. The total evaporation heat loss for Case 1 equals to that in the pre-flame zone (i.e. unburned zone),  $H_{all,1} = H_{ub}$ , while for Case 2,  $H_{all,2} = H_{ub} + H_b$ .

Fig. 7 shows the normalized evaporation heat loss  $H_{all,1}$  of propagating spherical flames for Case 1 at  $Le = 1$ . The corresponding flame propagating speed solutions are marked in Fig. 3a with the same symbols. The branches  $ab$  and  $a'b'$  respectively denote the stable flame solutions. It is seen that  $H_{all,1}$  first decreases sharply

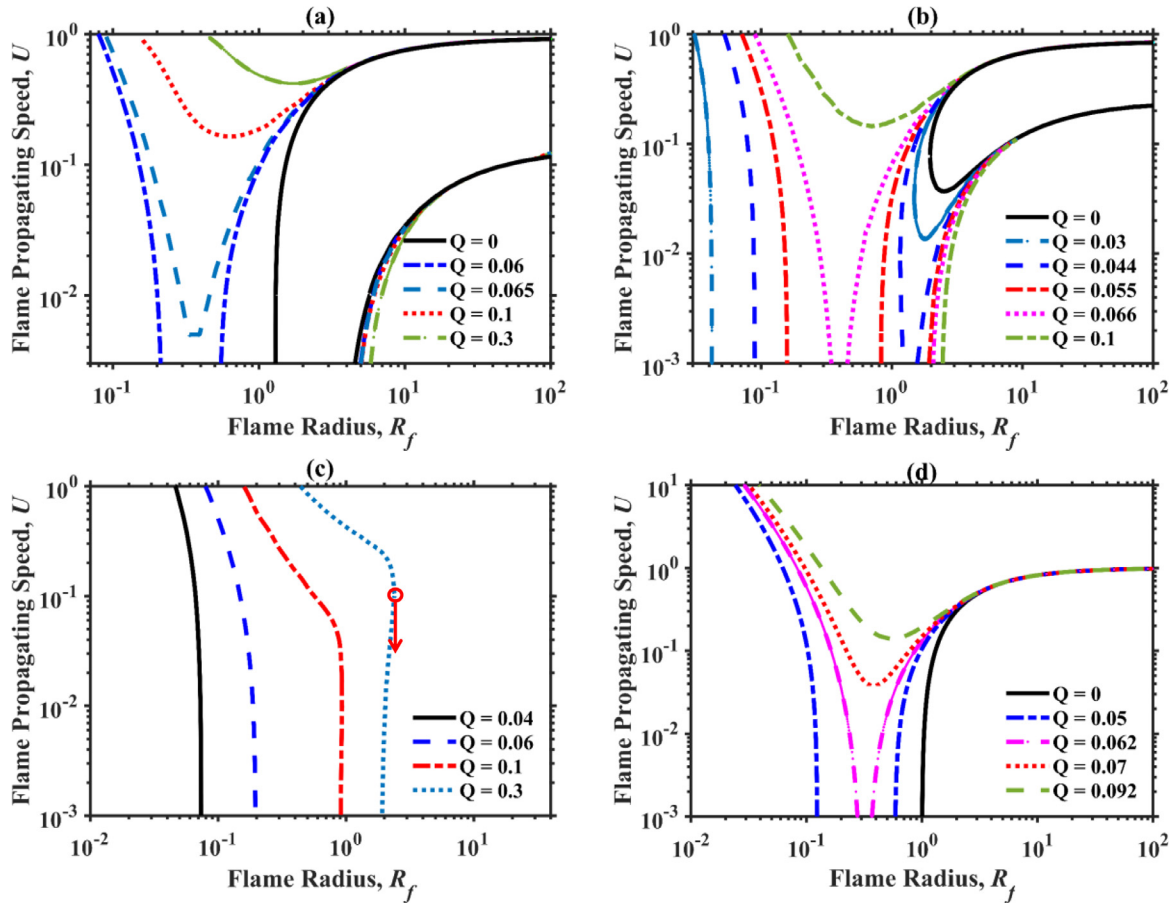


**Fig. 9.** Flame propagation speed as a function of flame radius with different ignition energies at  $Le = 1.0$ . The heat exchange coefficients considered are: (a)  $\Omega = 0.02$ , (b)  $\Omega = 0.04$ , (c)  $\Omega = 0.1$  and (d)  $\Omega = 0$ . The arrow in (c) indicates flame extinction.

and when  $R_f > 5$  their values are almost close to zero. This means that when the spherical flames stably propagate outwardly, the contributions from the droplet-induced heat loss diminish quickly and then they are almost neglected in the late stage of flame propagation. Also, lower  $\Omega$  leads to smaller  $H_{all,1}$  as shown in Fig. 7.

For Case 2, two flame regimes are selected here for further analysis: propagating spherical flame and SEF, as presented in Fig. 8a. Their flame propagating speed solutions have been given in Fig. 3b and the symbols in Fig. 8a are used to identify the same flame regimes in Fig. 3b. Along the travelling flame branch  $ab$ , the total heat loss  $H_{all,2}$  monotonically increases with the flame radius and at large radius (say  $R_f > 50$ ), it begins to drop. This is mainly due to the fact that total heat release from chemical reaction rather than heat loss of evaporation effect predominates as the flame grows. In SEF which appears with a greater  $\Omega$ , e.g. 0.026, the total heat loss  $H_{all,2}$  increases along the stable flame solutions  $a'c'b'$  and reaches its peak at point  $b'$ . As such, the flame extinguishment at point  $b'$  is caused by the droplet evaporation. Therefore, qualitatively, in Case 2 when the droplets lie at the full domain, the contributions from their evaporation shows different characteristics from those in Case 1.

Fig. 8b and c show the respective evaporation heat loss in Zone 2 and Zone 3, i.e.  $H_{ub}$  and  $H_b$ . When  $\Omega = 0.022$ , heat loss from the unburned zone  $H_{ub}$  (the stable branch  $a_1b_1$  in Fig. 8b) decreases sharply with increased flame radius, similar to what is observed from Case 1 in Fig. 7. However, for the contributions from the post-flame zone (i.e. burned zone),  $H_b$  (the stable branch  $a_2b_2$  in Fig. 8c) significantly increases when the flame propagates outwardly and then decreases as the cooling effect becomes weaker.

Besides, by comparing Fig. 8b and c, the higher total evaporation heat loss ( $H_{all,2}$ ) with larger flame radius is mainly caused by the droplet evaporation in the burned zone ( $H_b$ ). In SEFs,  $H_{ub}$  ( $a'_1c'_1b'_1$  in Fig. 8b) decreases monotonically and peaks at  $a'_1$ , while  $H_b$  ( $a'_2c'_2b'_2$  in Fig. 8c) increases monotonically and is highest at point  $b'_2$ . This also confirms the effects of the droplet evaporation in the post-flame zone.

#### 4.2. Spherical flame initiation

In this Section, we study initiation of droplet-laden spherical flames using an external energy flux ( $Q > 0$ ) at the spherical centre (Chen and Ju, 2007; Han and Chen, 2015; He, 2000; Zhang et al., 2013a; Zhang and Chen, 2011). The effects of droplet evaporation on the flame development (from ignition kernel, propagating spherical flame to planar flame) and minimum ignition energy with different Lewis numbers and heat exchange coefficients will be discussed in detail. Note that only Case 1 will be investigated here, as mentioned before in Section 2.2.

Fig. 9a shows the flame propagation speed as a function of flame radius at different ignition energies at  $Le = 1.0$  and  $\Omega = 0.02$ . Without ignition energy ( $Q = 0$ ), the result is the same as that in Fig. 3a, with stable (fast flame) and unstable (slow flame) branches. Once an external energy is deposited, the flame propagation trajectory is changed. Specifically, at low ignition energy, e.g.  $Q = 0.06$ , three branches are obtained. Besides the original stable and unstable branches, a new left ignition kernel branch at small radius arises. However, along it the flame is quenched at a flame ball solution. With increased  $Q$ , the ignition kernel branch and the middle

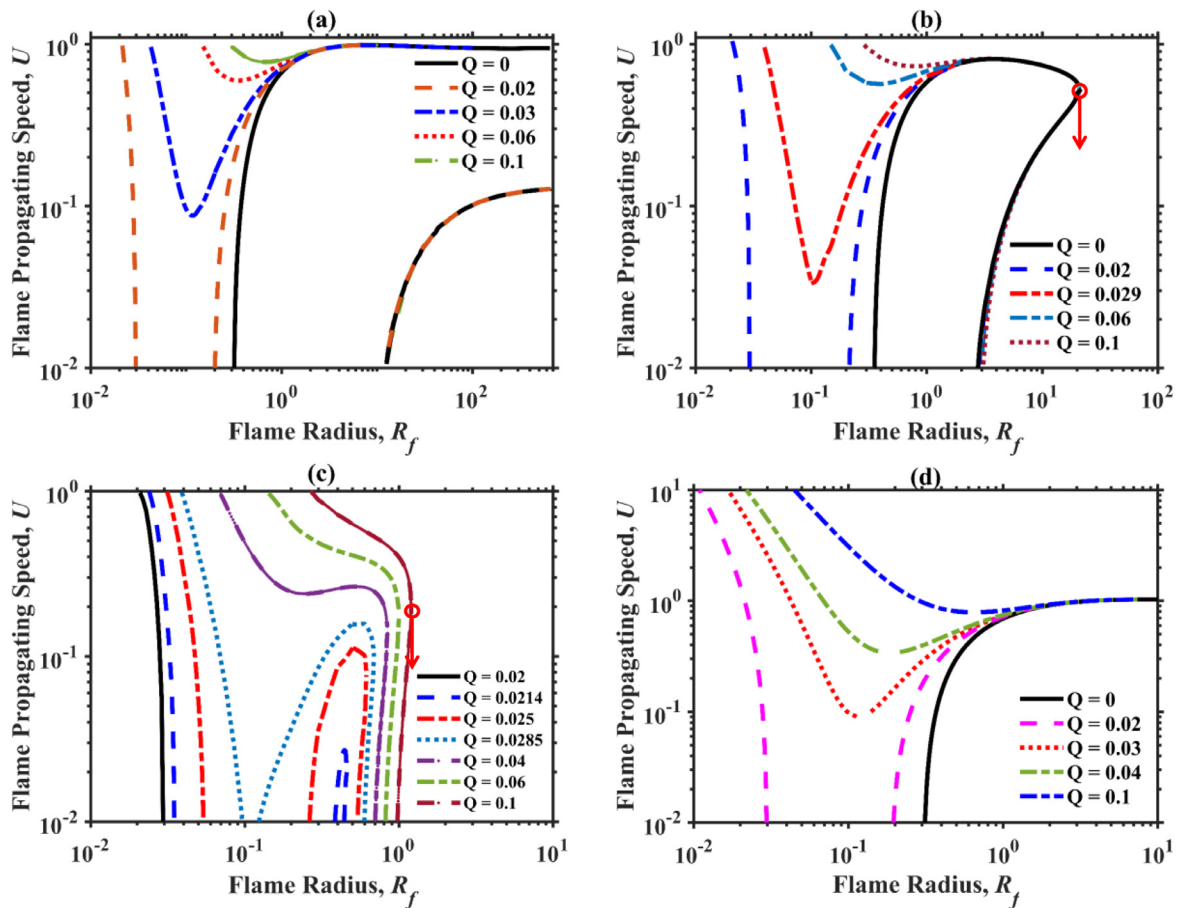


Fig. 10. Flame propagation speed as a function of flame radius with different ignition energies for Case 1 at  $Le=0.8$ . The heat exchange coefficients considered are: (a)  $\Omega=0.02$ , (b)  $\Omega=0.1$ , (c)  $\Omega=0.4$  and (d)  $\Omega=0$ . The arrows in (b) and (c) indicate flame extinction.

fast flame branch move towards each other. When  $Q$  is larger than a critical value  $Q_{min}=0.0637$ , these two branches merge, resulting in a travelling spherical flame branch, along which successful evolution of the flame kernel to self-sustaining propagating spherical flame can be achieved. The flame bifurcation from Fig. 9a was also observed from the previous theoretical analysis with one-step chemistry and two-step chemistry (Chen and Ju, 2007; He, 2000; Zhang and Chen, 2011).

For  $\Omega=0.04$ , Fig. 9b shows that only one C-shaped curve is observed for  $Q=0$ , same as that in Fig. 3a. When  $Q=0.03$ , a left flame kernel branch appears and the right C-shaped branch evolves slightly towards the left side. Further increasing  $Q$  to 0.044 makes the C-shaped branch break up into two branches (middle and right ones). However, successful ignition is still not achieved. Again, with  $Q$  is slightly higher than 0.066, successful ignition is achieved, in which case the ignition kernel and middle flame branches merge with each other. This leads to a new branch, along which the flame can propagate towards large radius. Therefore, the minimum ignition energy  $Q_{min}$  is 0.066, slightly greater than that in Fig. 9a.

However, for  $\Omega=0.1$ , Fig. 9c shows that there exists only one ignition kernel branch, however large the ignition energy  $Q$  is. For this case, the branch for outwardly propagating spherical flames degrades. At  $Q=0.04$ , along the ignition kernel branch, the flame propagation speed decreases sharply to zero (flame ball solutions) and the kernel is extinguished. When  $Q$  is further increased (say 0.3), the branch has a turning point, corresponding to the maximum possible flame radius. At that point, extinction occurs (indicated with an arrow in Fig. 9c) with finite flame propagating speed. This is new  $U-R_f$  pattern for extinction of ignition kernel and

not observed from the previous theoretical analysis in (Chen and Ju, 2007) for spherical flames with external heat loss. Therefore, the mixture with  $Le=1.0$  and  $\Omega=0.1$  is not ignitable with any ignition energies, since the mixture is essentially non-flammable. Comparing the results with droplets in Fig. 9a–c and without droplets in Fig. 9d, one can see the presence of the droplet considerably changes the relations between flame propagation speed and the radius. Also, the minimum ignition energy  $Q_{min}$  for gaseous flames is smallest ( $Q_{min}=0.0622$ ).

To compare the combined effects of evaporation heat loss and Lewis number, Fig. 10 shows the results for smaller Lewis number, i.e.  $Le=0.8$ . When  $\Omega=0.02$  in Fig. 10a, flame trajectories similar to those in Fig. 9a are observed. When  $\Omega=0.1$  in Fig. 10b, for  $Q=0$ , only sub-limit SEF can be observed, which is also shown in Fig. 4a. When  $Q=0.02$ , there are two branches: left ignition kernel and original sub-limit SEF. When  $Q$  is increased to minimum ignition energy  $Q_{min}=0.029$ , the flame kernel branch and the sub-limit SEF merge into one curve. Now the outwardly propagating spherical flame can be successfully initiated from the ignition kernel. Nevertheless, at around the turning point of sub-limit SEF (open circle in Fig. 10b), extinction occurs and the flame cannot propagate further towards ultimate planar flames. Therefore, overall, for this condition (i.e.  $Le=0.8$  and  $\Omega=0.1$ ), although the flame kernel can be initiated successfully, however, its development into large-radius spherical flames and further planar flames fails, even if the ignition energy is above the critical value, e.g. 0.06 and 0.1.

Fig. 10c shows  $U-R_f$  curves for the mixture with  $Le=0.8$  and  $\Omega=0.4$ . The mixture is not flammable (i.e. no propagating spherical flame solutions) when  $Q=0$ , based on Fig. 4a. When

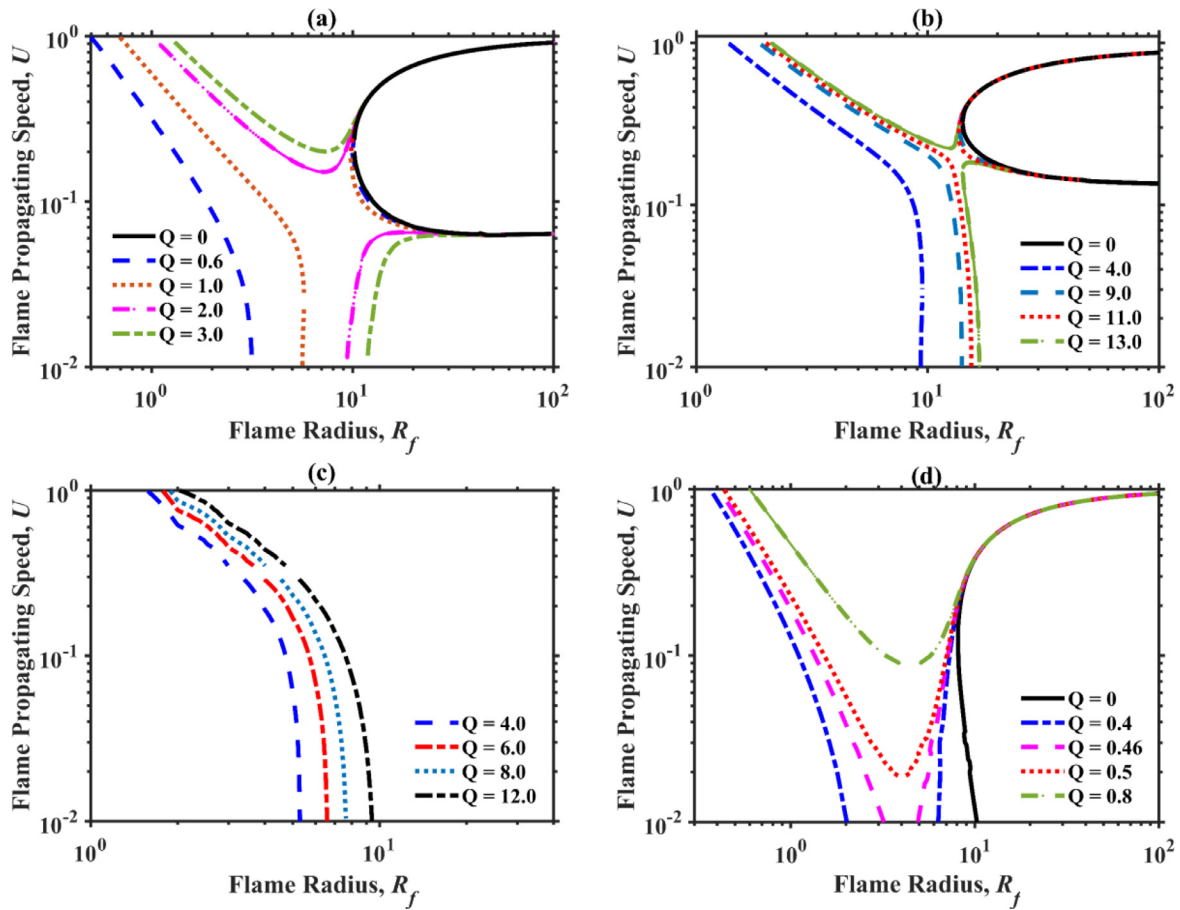


Fig. 11. Flame propagation speed as a function of flame radius with different ignition energies for Case 1 at  $Le = 1.5$ . The heat exchange coefficients considered are: (a)  $\Omega = 0.008$ , (b)  $\Omega = 0.02$ , (c)  $\Omega = 0.1$  and (d)  $\Omega = 0$ .

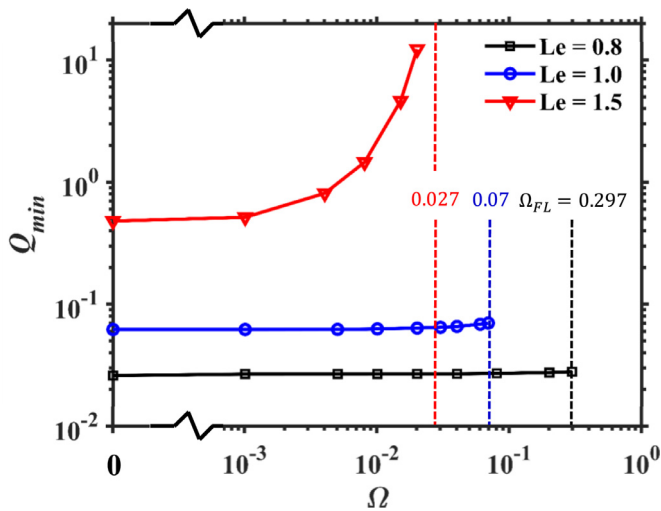


Fig. 12. Minimum ignition energy as a function of the heat exchange coefficient for  $Le = 0.8, 1.0$  and  $1.5$ .  $\Omega_{FL}$  is the maximum heat exchange coefficient for a flammable droplet-laden mixture.

$Q = 0.02$ , the left ignition kernel branch appears. A small increase in  $Q$  ( $= 0.0214$ ) leads to a new sub-limit SEF at intermediate radii, which is not seen in Fig. 9. As  $Q$  further increases, the ignition kernel branch merges with the stable flame branch of the sub-limit SEF, thereby reaching the critical ignition condition. At

larger ignition energies (e.g.  $Q \geq 0.04$ ), although they can successfully initiate the flames, it is always quenched at the turning points (open circle in Fig. 10c). This radius corresponding to extinction is generally smaller than those in Fig. 10b with  $\Omega = 0.1$ . Corresponding to the droplet-free situation, Fig. 10d shows that the similar trend with Fig. 10a, except without the right unstable (slow flame) branch, and as expected, its minimum ignition energy  $Q_{min}$  is smallest compared to those in Fig. 10a–c.

For  $Le = 1.5$ , Fig. 11a and b respectively show the  $U-R_f$  solutions with  $\Omega = 0.008$  and  $0.02$ . There are ignition kernel branches at small radii and propagating flame branches at large radii with low  $Q$  ( $\leq 1.0$  in Fig. 11a and  $\leq 11.0$  in Fig. 11b). However, unlike the results for  $Le = 0.8$  and  $1.0$ , the propagating flame branches in Fig. 11a and b are C-shaped. When  $Q$  is larger than a critical value (1.455 in Fig. 11a and 12.25 in Fig. 11b), two branches merge, resulting in upper fast flame and lower slow flame branches. A spherical flame can propagate outwardly along the fast flame branch, and hence a successful spherical flame initiation can be achieved. However, Fig. 11c shows that for  $\Omega = 0.1$ , the strong effect of water droplet evaporation makes the mixture become non-ignitable, similar to that in Fig. 9c and 10c. Like Figs. 9 and 10, the heat loss from the droplet evaporation has an important influence on spherical flame ignition, and the mixture without droplets is easiest to be ignited at a fixed  $Le$ .

Fig. 12 shows the minimum ignition energy  $Q_{min}$  as a function of the heat exchange coefficient  $\Omega$  for  $Le = 0.8, 1.0$  and  $1.5$ . The values of  $Q_{min}$  from droplet-free cases are also added for comparison. From Fig. 12, one can see that for increased Lewis num-

ber, the flammable range of  $\Omega$  ( $< \Omega_{FL}$ ) is greatly reduced, which can be identified by the left range of  $\Omega$  to the dashed lines in Fig. 12. Under the flammable condition, overall,  $Q_{min}$  increases with Lewis number. This was also observed by previous investigations in gaseous premixed spherical flames (Chen et al., 2011; Chen and Ju, 2007; Zhang and Chen, 2011). Meanwhile, the minimum ignition energy varies with  $\Omega$ , but the extent to which it, together with  $Le$ , affects  $Q_{min}$  is different. Specifically, for  $Le = 0.8$ ,  $Q_{min}$  is slightly affected by evaporation heat loss. The increase magnitude is about 4% when  $\Omega$  is changed from 0.001 to 0.297 in Fig. 12. For  $Le = 1.0$ ,  $Q_{min}$  increases by around 13% when  $\Omega$  increases from 0.001 to 0.07. For  $Le = 1.5$ ,  $Q_{min}$  increases significantly with  $\Omega$ , and when  $\Omega \geq 0.02$ , the mixture is very difficult to be ignited ( $Q_{min} > 10$ ).

## 5. Conclusions

In the present work, we develop a simplified theoretical model for premixed spherical flame initiation, propagation and extinction, considering two different distributions of dispersed water droplets. Correlations describing the flame propagation speed, flame temperature and vaporization front as functions of the flame radius at different heat exchange coefficients, Lewis numbers and ignition energies are derived. The results show that these correlations can describe different flame regimes and transitions among ignition kernels, flame balls, propagating spherical flames and planar flames. With the help of these correlations, the effects of water droplet evaporation on flame initiation, propagation and extinction are assessed.

The spherical flame propagation and extinction are strongly affected by heat exchange coefficients and Lewis numbers. With increased heat exchange coefficient, the flame propagation speed and flame temperature are reduced, while the distance between vaporization and flame fronts is increased. The various distributions of water droplets are compared (through Cases 1 and 2) and it is found that evaporation heat loss from the pre- and/or post-flame zones plays different roles in affecting flame propagation and extinction. As the flame propagates outwardly, the evaporation heat loss in the pre-flame zone decreases in both cases, while that from in post-flame zone in Case 2 firstly increases and then decreases when heat exchange coefficient is relatively small. In addition, the combined effects of stretch rate and Lewis number compete with the evaporation heat loss from droplet evaporation. For small Lewis number, the flammability limits for both cases can be achieved through self-extinguishing flames with large or intermediate stretch (small or intermediate radius), whereas for large Lewis number the flames approach their flammability limits under low stretch conditions (large flame radius).

For ignition of spherical flames, droplet evaporation and Lewis number considerably affect the ignition kernel formation and subsequent flame development. For flammable droplet-laden mixture, propagating spherical flames can be obtained with proper ignition energy deposition. If the mixture is intrinsically not flammable, although a flame kernel can be initiated, however it would still be quenched at an intermediate radius due to evaporation heat loss. At small Lewis number, the minimum ignition energy is slightly affected by droplet evaporation. However, it considerably increases with heat exchange coefficient for large Lewis number.

It should be highlighted that assumptions (e.g. constant thermal properties, quasi-steady state and dilute droplet concentration) are made here to perform the foregoing theoretical analysis. As such, the conclusions made above are valid only for the problems in which the above assumptions hold. In the future, further theoretical analysis through relaxing some of the above assumptions and/or detailed numerical simulations will be conducted to investigate initiation, propagation and extinction of propagating spherical flames laden with water droplets.

## Acknowledgements

Y.Z. is financially supported by Research Scholarship Budget from National University of Singapore (NUS). H.Z. is financially supported by the start-up grant (R-265-000-604-133) from NUS.

## References

- Belyakov, N.S., Babushok, V.I., Minaev, S.S., 2018. Influence of water mist on propagation and suppression of laminar premixed flame. *Combust. Theory Model.* 22, 394–409.
- Blouquin, R., Joulin, G., 1998. On the quenching of premixed flames by water sprays: influences of radiation and polydispersity. *Symp. Combust.* 27, 2829–2837.
- Cheikhbrat, H., Goulier, J., Bentaib, A., Meynet, N., Chaumeix, N., Paillard, C.E., 2015. Effects of water sprays on flame propagation in hydrogen/air/steam mixtures. *Proc. Combust. Inst.* 35, 2715–2722.
- Chelliah, H.K., 2007. Flame inhibition/suppression by water mist: droplet size/surface area, flame structure, and flow residence time effects. *Proc. Combust. Inst.* 31 (II), 2711–2719.
- Chen, Z., 2010. Effects of radiation and compression on propagating spherical flames of methane/air mixtures near the lean flammability limit. *Combust. Flame* 157, 2267–2276.
- Chen, Z., Burke, M.P., Ju, Y., 2011. On the critical flame radius and minimum ignition energy for spherical flame initiation. *Proc. Combust. Inst.* 33, 1219–1226.
- Chen, Z., Burke, M.P., Ju, Y., 2009. Effects of Lewis number and ignition energy on the determination of laminar flame speed using propagating spherical flames. *Proc. Combust. Inst.* 32 (I), 1253–1260.
- Chen, Z., Ju, Y., 2007. Theoretical analysis of the evolution from ignition kernel to flame ball and planar flame. *Combust. Theory Model.* 11, 427–453.
- Crowe, C.T., Schwarzkopf, J.D., Sommerfeld, M., Tsuji, Y., 2011. *Multiphase Flows with Droplets and Particles*, 2nd Edition CRC Press, Boca Raton.
- Dvorjetski, A., Greenberg, J.B., 2004. Theoretical analysis of polydisperse water spray extinction of opposed flow diffusion flames. *Fire Saf. J.* 39, 309–326.
- Dvorjetski, A., Greenberg, J.B., 2002. Analysis of extinction of counterflow polydisperse spray diffusion flames by a polydisperse water spray. *Proc. Combust. Inst.* 29, 385–392.
- Fuss, S.P., Chen, E.F., Yang, W., Kee, R.J., Williams, B.A., Fleming, J.W., 2002. Inhibition of premixed methane/air flames by water mist. *Proc. Combust. Inst.* 29, 361–368.
- Grant, G., Brenton, J., Drysdale, D., 2000. Fire suppression by water sprays. *Prog. Energy Combust. Sci.* 26, 79–130.
- Greenberg, J.B., 2007. Finite-rate evaporation and droplet drag effects in spherical flame front propagation through a liquid fuel mist. *Combust. Flame* 148, 187–197.
- Greenberg, J.B., Silverman, I., Tambour, Y., 1996. A new heterogeneous burning velocity formula for the propagation of a laminar flame front through a polydisperse spray of droplets. *Combust. Flame* 104, 358–368.
- Greenberg, J.B., Silverman, I., Tambour, Y., 1993. On the origins of spray sectional conservation equations. *Combust. Flame* 93, 90–96.
- Han, W., Chen, Z., 2016. Effects of finite-rate droplet evaporation on the extinction of spherical burner-stabilized diffusion flames. *Int. J. Heat Mass Transf.* 99, 691–701.
- Han, W., Chen, Z., 2015. Effects of finite-rate droplet evaporation on the ignition and propagation of premixed spherical spray flame. *Combust. Flame* 162, 2128–2139.
- Hayashi, S., Kumagai, S., 1975. Flame propagation in fuel droplet-vapor-air mixtures. *Symp. Combust.* 15, 445–452.
- He, L., 2000. Critical conditions for spherical flame initiation in mixtures with high Lewis numbers. *Combust. Theory Model.* 4, 159–172.
- Joulin, G., Clavin, P., 1979. Linear stability analysis of nonadiabatic flames: diffusional-thermal model. *Combust. Flame* 35, 139–153.
- Law, C.K., 2006. *Combustion Physics*. Cambridge University Press, New York.
- Lentati, A.M., Chelliah, H.K., 1998a. Physical, thermal, and chemical effects of fine-water droplets in extinguishing counterflow diffusion flames. *Symp. Combust.* 27, 2839–2846.
- Lentati, A.M., Chelliah, H.K., 1998b. Dynamics of water droplets in a counterflow field and their effect on flame extinction. *Combust. Flame* 115, 158–179.
- Li, H., Zhang, H., Chen, Z., 2018. Effects of endothermic chain-branching reaction on spherical flame initiation and propagation. *Combust. Theory Model* 1–19. In press.
- Mitani, T., 1982. A study on thermal and chemical effects of heterogeneous flame suppressants. *Combust. Flame* 44, 247–260.
- Mitani, T., 1981. A flame inhibition theory by inert dust and spray. *Combust. Flame* 43, 243–253.
- Modak, A.U., Abbud-Madrid, A., Delplanque, J.P., Kee, R.J., 2006. The effect of mono-dispersed water mist on the suppression of laminar premixed hydrogen-, methane-, and propane-air flames. *Combust. Flame* 144, 103–111.
- Naito, H., Uendo, T., Saso, Y., Kotani, Y., Yoshida, A., 2011. Effect of fine water droplets on extinguishment of diffusion flame stabilized in the forward stagnation region of a porous cylinder. *Proc. Combust. Inst.* 33, 2563–2571.
- Sakurai, I., Suzuki, J., Kotani, Y., Naito, H., Yoshida, A., 2013. Extinguishment of propane/air co-flowing diffusion flames by fine water droplets. *Proc. Combust. Inst.* 34, 2727–2734.
- Sasongko, M.N., Mikami, M., Dvorjetski, A., 2011. Extinction condition of counterflow diffusion flame with polydisperse water sprays. *Proc. Combust. Inst.* 33, 2555–2562.

- Sasongko, M.N., Seo, T., Mikami, M., 2016. Extinction condition of counterflow spray diffusion flame with polydisperse water spray. *Fire Saf. J.* 82, 23–29.
- Seshadri, K., 1978. Structure and extinction of laminar diffusion flames above condensed fuels with water and nitrogen. *Combust. Flame* 33, 197–215.
- Yang, W., Kee, J., R., 2002. The Effect of Monodispersed Water Mists on the Structure, Burning Velocity, and Extinction Behavior of Freely. *Combust. Flame* 130, 322–335.
- Yoshida, A., Kashiwa, K., Hashizume, S., Naito, H., 2015. Inhibition of counterflow methane/air diffusion flame by water mist with varying mist diameter. *Fire Saf. J.* 71, 217–225.
- Zegers, E.J.P., Williams, B.A., Sheinson, R.S., Fleming, J.W., 2000. Dynamics and suppression effectiveness of monodisperse water droplets in non-premixed counterflow flames. *Proc. Combust. Inst.* 28, 2931–2937.
- Zhang, H., Chen, Z., 2011. Spherical flame initiation and propagation with thermally sensitive intermediate kinetics. *Combust. Flame* 158, 1520–1531.
- Zhang, H., Guo, P., Chen, Z., 2013a. Critical condition for the ignition of reactant mixture by radical deposition. *Proc. Combust. Inst.* 34, 3267–3275.
- Zhang, H., Guo, P., Chen, Z., 2013b. Outwardly propagating spherical flames with thermally sensitive intermediate kinetics and radiative loss. *Combust. Sci. Technol.* 185, 226–248.